Resonant Ultrasound Spectroscopy Close to Its Applicability Limits

Michal LANDA[a], Hanuš SEINER[a,b], Petr SEDLÁK[a,b],
Lucie BICANOVÁ[a,b], Jan ZÍDEK[a], Luděk HELLER[a]

[a]Institute of Thermomechanics v.v.i., Academy of Sciences of Czech Republic,
Dolejškova 5, 18200 Prague 8, Czech Republic
[b]Faculty of Nuclear Sciences and Physical Engineering, Czech Technical University in
Prague, Trojanova 13, 12000 Prague 2, Czech Republic

ABSTRACT – This chapter brings a critical review of the applicability of the resonant ultrasound spectroscopy (RUS) for determination of all independent elastic coefficients of anisotropic solids. Such applicability limits are sought which follow from the properties of the examined materials, i.e. from the strength and class of the anisotropy, etc.. After introducing the general theoretical background of RUS, particular limiting factors are illustrated on experimental results, namely on the investigation of extremely strongly anisotropic single crystals, of weakly anisotropic polycrystals (where neither the class nor the orientation of the anisotropy are known) and of single crystals with strong temperature-dependent magneto-elastic attenuation. In all these cases, a sensitivity analysis is carried out to show which elastic coefficients (their combinations) can be accurately determined form RUS measurements and which cannot, whereto the complementarity of the RUS and pulse-echo methods is shown and utilized. The general findings of both the theoretical introduction and the experimental part are summarized in a concluding section, which tries to formulate the most essential open questions of the RUS method.

1 Introduction

Although the fundamentals of resonant ultrasound spectroscopy (RUS) are known to the physics community for more than fifteen years [1, 2], this method cannot still be counted among well established or routinely used experimental techniques for evaluation of elastic properties of anisotropic solids. In comparison with methods based on acoustic wave velocity measurements, as are the family of pulse-echo techniques (either contact or with immersion in a liquid), point-source/point-receiver (PS/PR) or surface acoustic waves (SAW) methods, the employment and the scientific impact of RUS are undoubtedly minor, except

of some cases where e.g. measurements in wide ranges of temperatures are required [3–5] which disqualifies the above more conventional methods because of technical difficulties.

The reason why such reliable and accurate method finds only hardly its way into a broader awareness could be sought neither in requirements on the tested specimens (RUS has been already successfully applied to prisms [1, 2], plates [6], membranes [7], spherical balls [8], cylindrical nanotubes [9], rods [10], or samples of even more general shapes [11]) nor in requirements on the experiment instrumentation. The problem lies in the *inverse procedure*, i.e. in the procedure necessary to obtain the desired information (the elastic coefficients) from the experimental data. Whereas the pulse-echo measurements result in sets of ultrasound velocities in various directions, indicating clearly and understandably the anisotropy of the material, the outputs of RUS (resonant spectra of mechanical vibrations of a chosen specimen) require a sophisticated postprocessing to reveal the information on the material encrypted in it. This inverse procedure cannot be constructed universally, once for ever – each particular application of RUS requires slight modification of the procedure, taking the geometry of the specimen, strength of the anisotropy or the attenuation in the material into account. That is the reason why the RUS techniques appear to be unsuitable for automation, and thus, for massive use in commercial devices, industry or applied research.

This chapter aims to bring an analysis of what the applicability limits of RUS can be, searching for the novel ways how the inverse procedures can be constructed to push these limits at least a tiny bit further. It focuses on the limits given by the nature of the method itself, rather than these resulting from the experimental setup, although some such problems are mentioned as well. In the first half of this chapter, general ideas of the RUS method is overviewed with special emphasis laid on the relation between the properties of the examined material and the information obtainable on them by RUS measurements. The essentiality of the knowledge of such relations is revealed in the second half of the chapter, where the RUS method is applied to particular issues from solid state physics and materials science.

2 Resonant ultrasound spectroscopy - a general background

2.1 Historic development of RUS

The fact that the resonant spectra of free vibrations of a homogeneous, elastically anisotropic, rectangular parallelepiped contain a sufficient information on the elastic anisotropy of the material became fully understood in the first half of 1970s by Demarest et al. [13]. After significant extensions by Ohno [14], this finding has found a broad applicability in geophysics, which, according to [15], motivated Migliori et al. [2] to develop a similar method for investigation of elastic properties of small crystalline samples, and introduce, thus, these approaches to the general physics community. As the resonant frequencies of such small specimens were in the ultrasonic domain, Migliori et al. decided to refer this new method to as the *resonant ultrasound spectroscopy* (abbreviated as RUS), which was an equivalent of the term *rectangular parallelepiped resonance method* (RPR)

used in geophysics.

The main idea of RUS was following: Let us consider that the first n resonant frequencies ($f_{p=1\ldots n}$) of free elastic vibrations of a small rectangular parallelepiped of the examined material are obtained experimentally. Then, let us construct a numerical procedure which for every guess of elastic coefficients c_{ij} calculates an estimate of the first n resonant frequencies of such rectangular parallelepiped ($f^{\text{calc.}}_{p=1\ldots n}(c_{ij})$). By matching the experimental and calculated frequencies, i.e. by minimizing the difference

$$\Delta(c_{ij}) = \sum_{p=1}^{n} \left(f_p - f_p^{\text{calc.}}(c_{ij})\right)^2 \tag{1}$$

over all c_{ij}, one can easily reach the coefficients which describe the vibrational properties (and, consequently, the elasticity) in some 'optimal' way.

For the numerical calculation of the vibrational modes for given c_{ij}, Migliori et al. overtook the original RPR algorithm and used a variational (Rayleigh-Ritz) method. For the consequent minimization of (1), a gradient search routine was adopted. During the next fifteen years, this basic scheme of the inverse method remained nearly unchanged. The only significant improvement came from Ogi et al. [17], who proposed to identify particular modes of vibrations by scanning the surface of the specimen by a laser interferometer during the measurements. This mode identification enabled a correct association of the pairs of resonant frequencies (the measured and the calculated) appearing in (1), which stabilized significantly the minimization procedure. The RUS methods with such mode identification became later called *modal resonant ultrasound spectroscopy* (MRUS) to emphasize the role of the shapes of the vibrational modes played in the inverse procedure.

The RUS method was successfully tested on known materials (namely $SrTiO_3$ in [2]) and immediately applied for determination of the elastic properties of advanced materials, such as high-temperature superconductors [2, 18, 19], or quasicrystals [20, 21], where both the need of measurements in extremely low temperatures and the small dimensions of the obtainable specimens precluded the use of the pulse-echo methods. Along with the application of RUS for particular materials, the method itself became more and more general. Whereas the use of the original algorithm described in [2] was restricted to a rectangular parallelepiped cut exactly along the principal axes of an orthorhombic (or higher) symmetry, Sarrao et al. [16] have shown soon that the method can be also used for identification of the crystallographic orientation of the material anisotropy inside the specimen. In the widely cited paper [15], Maynard writes about the applicability of the RUS method to 'prisms, spheroids, ellipsoids, shells, bells, eggs, potatoes, sandwiches and other shapes', meaning that the inverse procedure can be easily modified for any geometrically well-defined shape. However, the first successful attempts to use RUS for investigation of thin films and coatings came about ten years later [22–24].

In the most recent applications, the outputs of RUS are often not restricted to the elastic coefficients only. The results of the RUS measurements could be also the piezoelectric constants [25] or the internal friction parameters [26], or both [27]. Moreover, the changes in the resonant spectra can simply serve as reliable indicators of damage in the material

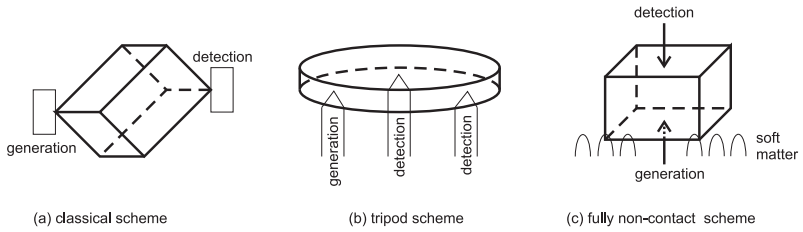

Figure 1: The main experimental schemes of RUS: The classical scheme, the tripod scheme and the fully non-contact scheme.

[28–30]. The main idea of the method, however, remains nearly the same, always consisting of measurements of the resonant spectra and, consequently, of the analysis of these spectra by an inverse algorithm.

For completeness, let us here also summarize the recent development in the experimental part of RUS, i.e. the methodology how the resonant spectra are experimentally obtained. Three principally different experimental arrangements of RUS measurements can be found in the available literature (Fig. 1):

1. The **classical scheme** was adopted by the pioneering works in RUS and remained as a most widely used RUS experimental methodology till nowadays. This scheme follows the setups used in the RPR measurements in geophysics. In Fig.1(a), the main idea of this scheme is outlined: The specimen (parallelepiped, sphere, or any other bulk shape) is placed between two transducers such that the contact area between the specimen and the transducers is minimal (e.g. a cube is placed such that it touches the transducers by two opposite corners only) to ensure the best possible approximation of fully free vibrations. Then, one of the transducers is used as a generator of ultrasonic waves (either scanning slowly the frequencies within a chosen range, or generating a broadband pulse), whereas the second as a detector. Obviously, the main disadvantage of such method lies in the fact that the vibrations are not purely free, as the specimen is restricted by the contact forces from the transducers. This effect was repeatedly shown to be negligible [33, 34], but for the bulk specimens only. For thin plates or shells, which have bending stiffness in some directions comparable to the forces applied by the contact of the transducers, the classical scheme becomes unsuitable.

   As mentioned above, the classical scheme can be significantly improved by scanning the specimen by a laser vibrometer during the measurements in order to obtain the shapes of particular eigenmodes.

2. The **tripod scheme** solves the problem of contact forces for thin plates. First adopted by Ogi [17], this scheme uses the arrangement outlined in Fig.1(b). The contact forces are minimized to the gravitation of the specimen lying of a tripod of rod-like transducers. Alternatively, either all the rods can be transducers, one used as a gener-

ator, the other two detecting the vibrations, or one of the rods can be just supporting the specimen and the remaining two be the generator and detector. Another crucial advantage of the tripod scheme is that the rods can be the waveguides only, transmitting the ultrasonic signal to/from the specimen from/to the piezoelectric transducers situated relatively far away from the specimen. This enables the tripod scheme to be used for measurements at extreme temperatures with the transducers (which are temperature-sensitive as well) situated safely outside the furnace or the cryostat [35].

Again, the tripod scheme can be improved by detecting the modes of vibrations.

3. The **fully non-contact scheme** (Fig.1(c)) is a logical extension of the tripod. In this arrangement, the specimen is not laid on a firm tripod but either hung on thin wires (glued to two 250μm wires using a minimal amount of Torr-seal epoxy in [36]) or laid on a soft underlay made of a material with extremely low acoustic impedance (cork wood used in most of the results presented by the authors within this chapter). The vibrations here are both generated and detected by lasers, the contact with the transducers is fully avoided. It is more than natural that the mode identification can be easily implemented in this scheme. The fully non-contact arrangement seems also to be optimal for the use at elevated or low temperatures.

   There is, however, another way how to perform RUS experiments in a fully non-contact regime. It is the *electromagnetic acoustic resonance method (EMAR)* [37], where a solenoidal coil and a static magnetic field are used to induce a induce Lorentz forces on specimen surfaces without using any mechanical contacts. More over, this is method sometimes called mode-selective, which means that particular sets of vibration modes can be selectively excited and detected by changing the direction of the applied magnetic field. The EMAR measurements are, on the other hand, fully dependent on the conductivity and other electromagnetic properties of the tested specimen, and cannot be counted among general experimental techniques of RUS.

All the experimental data presented in this chapter were obtained by the fully non-contact RUS technique. The elastic vibrations in the specimen were excited by sequences of pulses of an unfocused infrared laser beam (Nd:YAG, General Photonics Corporation TWO-45Q, nominal wavelength 1064nm) from the side of the specimen. The vibrations were recorded by scanning red-light laser vibrometer (Polytec OFV-2570 equipped by a scanning unit consisting of two dielectric mirrors on motorized positional stages) on the upper surface of the specimen.

2.2 The forward problem

The term *forward problem of RUS* is, in general, used for the evaluation of eigenfrequencies and eigenmodes of free vibrations of an elastic specimen of given geometry and known elastic coefficients. To solve the forward problem, the natural starting point is to formulate the energetic quantities of a dynamically deformed elastic specimen. For given displacement field $\mathbf{u}(\mathbf{x},t)$ and its time derivative $\dot{\mathbf{u}}(\mathbf{x},t)$, and for given density ρ and the elastic

coefficients C_{ijkl}, these quantities are: the kinetic energy

$$K(\dot{\mathbf{u}}(\mathbf{x},t),t) = \frac{1}{2}\int_V \rho \dot{u}_i \dot{u}_i \mathrm{d}V, \tag{2}$$

the potential (stored, elastic) energy

$$P(\mathbf{u}(\mathbf{x},t),t) = \frac{1}{2}\int_V C_{ijkl}\frac{\partial u_i}{\partial x_j}\frac{\partial u_k}{\partial x_l}\mathrm{d}V, \tag{3}$$

and the Lagrangian energy

$$L(\mathbf{u}(\mathbf{x},t),\dot{\mathbf{u}}(\mathbf{x},t),t) = K(\dot{\mathbf{u}}(\mathbf{x},t),t) - P(\mathbf{u}(\mathbf{x},t),t), \tag{4}$$

which is their difference. All the volumetric integrations are meant over the whole volume of the specimen V.

As we are searching for harmonic solutions (eigenvibrations), an assumption about the form of the displacement field can be done by stating

$$\mathbf{u}(\mathbf{x},t) = \mathbf{u}(\mathbf{x})\cos(\omega t) \qquad \text{and} \qquad \dot{\mathbf{u}}(\mathbf{x},t) = -\mathbf{u}(\mathbf{x})\sin(\omega t). \tag{5}$$

This simplifies the Lagrangian energy into

$$L(\mathbf{u}(\mathbf{x}),t) = \frac{1}{2}\int_V \left[\omega^2 \rho u_i u_i \sin^2(\omega t) - C_{ijkl}\frac{\partial u_i}{\partial x_j}\frac{\partial u_k}{\partial x_l}\cos^2(\omega t)\right]\mathrm{d}V. \tag{6}$$

One of the basic properties of the Lagrangian energy is that it follows stationary paths between each two given time points[1]. In our case of $L = L(\mathbf{u}(\mathbf{x}),t)$ it means that

$$\delta\int_{t_1}^{t_2} L(\mathbf{u}(\mathbf{x}),t)\mathrm{d}t = \int_{t_1}^{t_2} L(\mathbf{u}(\mathbf{x})+\delta\mathbf{u}(\mathbf{x}),t)\mathrm{d}t - \int_{t_1}^{t_2} L(\mathbf{u}(\mathbf{x}),t)\mathrm{d}t = 0, \tag{7}$$

for arbitrary but given t_1 and t_2, where $t_1 < t_2$. By choosing these time points such that $t_2 = t_1 + 2\pi/\omega$, and taking the equality

$$\int_0^{2\pi/\omega}\cos^2(\omega t) = \int_0^{2\pi/\omega}\sin^2(\omega t) \tag{8}$$

into account, the time coordinate can be simply eliminated, and we arrive another variational condition:

$$0 = \delta\frac{1}{2}\int_V \underbrace{\left[\omega^2\rho u_i u_i - C_{ijkl}\frac{\partial u_i}{\partial x_j}\frac{\partial u_k}{\partial x_l}\right]}_{\overset{\text{def.}}{=}\lambda(\mathbf{u}(\mathbf{x}))}\mathrm{d}V \overset{\text{def.}}{=} \delta\Lambda(\mathbf{u}(\mathbf{x})), \tag{9}$$

[1] So-called *principle of stationary (or minimal) Lagrangian action* or *Hamiltonian principle*, e.g. [31].

where we have defined two new quantities: the *time-averaged Lagrangian energy* $\Lambda(\mathbf{u}(\mathbf{x}))$ and its density $\lambda(\mathbf{u}(\mathbf{x}))$. Following the basic theorems of the calculus of variation, we can express the variation of $\Lambda(\mathbf{u}(\mathbf{x}))$ explicitly as

$$\delta\Lambda(\mathbf{u}(\mathbf{x})) = \frac{1}{2}\int_V \left[\frac{\partial\lambda}{\partial u_i} - \frac{\mathrm{d}}{\mathrm{d}x_j}\left(\frac{\partial\lambda}{\partial(\frac{\partial u_i}{\partial x_j})}\right)\right]\delta u_i \mathrm{d}V + \int_S n_j \frac{\partial\lambda}{\partial(\frac{\partial u_i}{\partial x_j})}\delta u_i \mathrm{d}S, \tag{10}$$

where S is the surface of the specimen and $\mathbf{n}$ its outer normal. As the variations δu_i are arbitrary, we can require that

$$\frac{\partial\lambda}{\partial u_i} - \frac{\mathrm{d}}{\mathrm{d}x_j}\left(\frac{\partial\lambda}{\partial(\frac{\partial u_i}{\partial x_j})}\right) = \rho\omega^2 u_i + C_{ijkl}\frac{\partial^2 u_k}{\partial x_j \partial x_l} = 0 \qquad \text{almost everywhere in } V \tag{11}$$

$$\text{and} \qquad n_j \frac{\partial\lambda}{\partial(\frac{\partial u_i}{\partial x_j})} = n_j C_{ijkl}\frac{\partial u_k}{\partial x_l} = 0 \qquad \text{almost everywhere on } S. \tag{12}$$

Obviously, (11) are the equations of steady waves in the considered continuum and (12) are the conditions of a free surface. Thus, by $\delta\Lambda = 0$, we obtain the solutions of the elastodynamic equation (11) for boundary conditions (12), which is exactly what we are searching for – resonant vibrations of an unconstrained specimen.

Let us now try to construct a displacement field $\mathbf{u}(\mathbf{x})$ such that it minimizes $\Lambda(\mathbf{u}(\mathbf{x}))$. If the specimen is, for example, a rectangular parallelepiped of dimensions $d_1 \times d_2 \times d_3$, the Lagrangian is

$$\Lambda = \frac{1}{2}\int_{-d_1/2}^{d_1/2}\int_{-d_2/2}^{d_2/2}\int_{-d_3/2}^{d_3/2}\left[\rho\omega^2 u_i^2(\mathbf{x}) - C_{ijkl}\frac{\partial u_i}{\partial x_j}(\mathbf{x})\frac{\partial u_k}{\partial x_l}(\mathbf{x})\right]\mathrm{d}x_1\mathrm{d}x_2\mathrm{d}x_3, \tag{13}$$

where the coordinate system $\mathbf{x}$ was chosen such that it has its origin in the center of the specimen and that the edges of lengths d_1, d_2 and d_3 are oriented along the axes x_1, x_2 and x_3. As utilized by the original RPR algorithm [13] and adopted by the pioneering works of RUS [1, 2], the variation of this Lagrangian with respect to $\mathbf{u}(\mathbf{x})$ can be approximated by derivatives of it with respect to the coefficients of polynomial expansions of $\mathbf{u}(\mathbf{x})$ (so-called variational Ritz method). In the other words, for the solution expected in an approximative form

$$u_i(\mathbf{x}) = \sum_{K=1}^{N} \alpha_{[K,i]}\Psi_K(\mathbf{x}), \tag{14}$$

where $\Psi_K(\mathbf{x})$ is some properly chosen functional (e.g. polynomial) basis, the condition $\delta\Lambda(\mathbf{u}(\mathbf{x})) = 0$ is satisfied whenever

$$\frac{\partial\Lambda(\alpha_{[1,1]},\ldots,\alpha_{[N,1]},\alpha_{[1,2]},\ldots,\alpha_{[N,2]},\alpha_{[1,3]},\ldots,\alpha_{[N,3]})}{\partial\alpha_{[K,i]}} = 0 \tag{15}$$

for all $[K,i] \in [\{1,2,\ldots,N\},\{1,2,3\}]$

Although *any* polynomial basis (e.g. $\Psi_{abc} = x_1^a x_2^b x_3^c$ used in [2]) could be suitable for such approximation, it is advantageous here, for the case of the rectangular parallelepiped with mutually comparable dimensions, to take [17]

$$\Psi_{abc} = P_a(\frac{2x_1}{d_1})P_b(\frac{2x_2}{d_2})P_c(\frac{2x_3}{d_3}) \tag{16}$$

for

$$a,\, b,\, c = 0, 1, 2, 3 \ldots \qquad\qquad a + b + c \leq N, \tag{17}$$

where $P_n(x)$ is the normalized Legendre polynomial of degree n defined as

$$P_n(x) = \frac{\sqrt{(2n+1)/2}}{2^n n!} \left[\frac{\mathrm{d}^n}{\mathrm{d}x^n}(x^2 - 1)^n \right]. \tag{18}$$

The corresponding stationary condition for Lagrangian Λ leads to a symmetric eigenvalue problem

$$\left(\omega^2 \mathbf{E}_{[abc,i][def,j]} - \Gamma_{[abc,i][def,j]}\right) \alpha_{[abc,i]} = 0, \tag{19}$$

with

$$\mathbf{E}_{[abc,i][def,j]} = \delta_{ij}\delta_{ad}\delta_{be}\delta_{cf}, \tag{20}$$

and

$$\Gamma_{[abc,i][def,j]} = \frac{1}{\rho}\frac{8}{d_1 d_2 d_3} C_{ijkl} \int_{-d_1/2}^{d_1/2} \int_{-d_2/2}^{d_2/2} \int_{-d_3/2}^{d_3/2} \frac{\partial \Psi_{abc}}{\partial x_k} \frac{\partial \Psi_{def}}{\partial x_l} \mathrm{d}x_1 \mathrm{d}x_2 \mathrm{d}x_3. \tag{21}$$

Let it be pointed out that for a general polynomial basis, the matrix $\mathbf{E}$ is not unitary, which significantly complicates the solution of the eigenvalue problem.

The integrations in matrix Γ can be done analytically (using a symbolic software) and the eigenvalue problem for this matrix is usually solved by an appropriate numerical algorithm (e.g. the Cholesky method [32]).

Three remarks are to be done here before proceeding to the description of the inverse procedure:

1. For reasonably precise polynomial approximation (14), the matrices Γ are huge and their construction by (21) consumes unacceptable portions of the computation time if it must be done again and again during the optimizing process. For this reason, it is beneficial to notice that this matrix is linearly dependent on C_{ijkl}, regardless of how nontrivial this dependence is.

   Consequently, the derivatives $\partial\Gamma_{mn}/\partial C_{ijkl}$ are independent on C_{ijkl} and can be computed *a priori*. In each run of the optimizing process, the matrix Γ can be, thus, quickly constructed as

$$\Gamma_{mn} = \sum_{ijkl} \frac{\partial \Gamma_{mn}}{\partial C_{ijkl}} C_{ijkl}. \tag{22}$$

The summation here is carried only over the independent elastic coefficients C_{ijkl}, which means that e.g. for the cubic symmetry the matrices Γ are always obtained as linear combinations of three matrices: $\partial\Gamma/\partial c_{11}$, $\partial\Gamma/\partial c_{12}$ and $\partial\Gamma/\partial c_{44}$.

2. The above described algorithm for solution of the forward problem can be easily modified for a nonrectangular parallelepiped by transforming the Lagrangian (13) into an oblique coordinate system chosen paraxially with the edges of the specimen. For such oblique system $\mathbf{y}$ related to the natural system of the anisotropy $\mathbf{x}$ by a linear relation

$$\mathbf{y} = \mathbf{B}\mathbf{x}, \tag{23}$$

the Lagrangian transforms into [49]

$$\Lambda = \frac{1}{2}\int_{-d_1/2}^{d_1/2}\int_{-d_2/2}^{d_2/2}\int_{-d_3/2}^{d_3/2}\left[\frac{\rho}{\det\mathbf{B}}\omega^2 u_i^2(\mathbf{y}) - T_{ijkl}\frac{\partial u_i}{\partial y_j}(\mathbf{y})\frac{\partial u_k}{\partial y_l}(\mathbf{y})\right]\mathrm{d}y_1\mathrm{d}y_2\mathrm{d}y_3, \tag{24}$$

where

$$T_{ijkl} = \frac{1}{\det\mathbf{B}}C_{ipko}B_{jp}B_{lo}. \tag{25}$$

As expressions (13) and (24) are formally identical, the eigenfrequencies of a general parallelepiped can be then evaluated using exactly the same variational procedure as for the rectangular one.

3. The direct problem can be significantly simplified by the symmetry. If the specimen is, for example, a rectangular parallelepiped cut exactly along the principal axes of an orthorhombic (or higher) symmetry, the variational problem (9) has an orthorhombic symmetry, which is the highest common symmetry of the specimen and the material. Consequently, the solutions (eigenmodes) can be expected to inherit this class of symmetry, as they fulfill the new balance laws following from it (according to the Noether's principle). In such case, it is clear that the functions $u_i(\mathbf{x})$ must be either even or odd with respect to all cartesian coordinates x_j with (in contrary) either odd or even partial derivatives $\partial u_i/\partial x_j$. The overall vibrations of such specimen can be, thus, fully characterized by displacement fields in the octant $[0, d_1/2] \times [0, d_2/2] \times [0, d_3/2]$. The way how can this symmetry be utilized for in the numeric calculation of the eigenfrequencies and eigenmodes is in detail discussed in [2], where the matrix Γ is shown to split into eight independent matrices, each one corresponding to one possible symmetry of the resultant vibrational modes.

   There is, moreover, another consequence of such symmetry of the specimen, which is perhaps even more important that the simplification of the forward problem. Consider, for example, an even mode of vibrations, where (for all i)

$$u_i(x_1 = \frac{d_1}{2}, x_2, x_3) = u_i(x_1 = -\frac{d_1}{2}, x_2, x_3),$$

$$u_i(x_1, x_2 = \frac{d_2}{2}, x_3) = u_i(x_1, x_2 = -\frac{d_2}{2}, x_3),$$

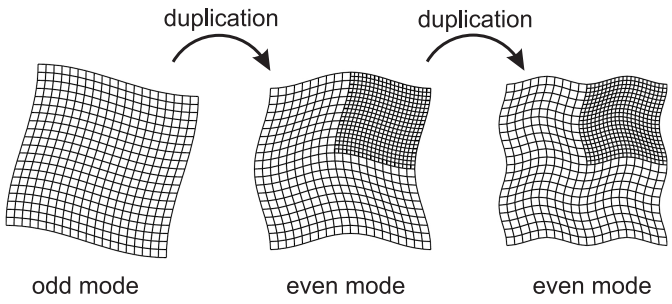

Figure 2: Construction of higher modes of free vibrations by duplication (a 2D model). The initial odd mode is duplicated into an even one by choosing proper phases of the mode in particular quadrants. Further duplication results in the even modes, which are obtained without any phase changes.

$$u_i(x_1, x_2, x_3 = \frac{d_3}{2}) = u_i(x_1, x_2, x_3 = -\frac{d_3}{2}), \tag{26}$$

and let this mode correspond to the eigenfrequency ω. Then, another mode can be easily constructed by duplication, i.e. by taking

$$\mathbf{u}^D(\frac{1}{2}\mathbf{x}) = \mathbf{u}\left(\mathbf{x} - [\frac{d_1}{2}, \frac{d_2}{2}, \frac{d_3}{2}]\right), \tag{27}$$

in the first octant (i.e. in $[0, d_1/2] \times [0, d_2/2] \times [0, d_3/2]$), and by periodic repetition of this displacement field in the remaining seven eights of the specimen. The duplicated mode obviously fulfills the variational condition (11) for the eigenfrequency $\omega^D = 2\omega$. Similarly, the input even mode (26) can be triplicated with frequency 3ω, quadruplicated with 4ω, or generally n-multiplied with frequency $n\omega$. Such multiplication procedure can be done also for odd modes, where

$$\begin{aligned} u_i(x_1 = \frac{d_1}{2}, x_2, x_3) &= -u_i(x_1 = -\frac{d_1}{2}, x_2, x_3), \\ u_i(x_1, x_2 = \frac{d_2}{2}, x_3) &= -u_i(x_1, x_2 = -\frac{d_2}{2}, x_3), \\ u_i(x_1, x_2, x_3 = \frac{d_3}{2}) &= -u_i(x_1, x_2, x_3 = -\frac{d_3}{2}), \end{aligned} \tag{28}$$

or for any mode being alternatively even or odd in individual cartesian coordinates x_i, as it follows from the symmetry of the system with respect to mirror reflections $x_i \to -x_i$ valid in the considered orthorhombic specimen. The difference between the duplication for the even and the odd modes is shown in Fig.2. To summarize, we can say that with each mode of frequency ω, the spectrum of an rectangular specimen aligned with the orthorhombic symmetry of the material contains also all multiplications of this frequency. In the case of generally oriented or non-rectangular parallelepipeds, no such general conclusion can be done. However, whenever the

specimen has a shape suitable for spatial repetition, there can be some modes able to be multiplied within the spectrum.

2.3 Inverse determination of elastic coefficients

As it was already mentioned, the inverse procedure is the key point of the all RUS techniques. Within this procedure, the aim is to determine the unknown elastic coefficients, and what we have on disposal are the experimentally obtained resonant spectra and a numerical algorithm for solution of the forward problem.

The obvious way how to obtain the optimal elastic coefficient is to minimize the difference (1) or any nondecreasing function of it. Migliori et al. [2] used

$$\Delta(c_{ij}) = \sum_{p=1}^{n} \frac{\left(f_p - f_p^{\text{calc.}}(c_{ij})\right)^2}{f_p^2}, \tag{29}$$

which reflects the fact that the higher frequencies are due to the approximation (16) less accurately determined and are, thus, involved in (29) with lower weights.

Let us see now how easily can this natural weighting turn into a drawback. Let us consider that our specimen is a thin cylindrical rod made of oak wood (cut along the grain), and let us admit such rod to vibrate both in the longitudinal and the torsional regime (but not in the flexural modes). For the longitudinal vibrations, the steady wave equation (11) can be written as

$$\rho\omega^2 u + E\frac{\mathrm{d}^2 u}{\mathrm{d}x^2} = 0, \tag{30}$$

where u is the axial displacement field and E is the Young modulus in the axial direction of the rod, whereas for the torsional vibrations as

$$\rho\omega^2 \theta + G_\perp \frac{\mathrm{d}^2 \theta}{\mathrm{d}x^2} = 0, \tag{31}$$

where θ is the torsion angle and $G_\perp$ is the shear modulus for shears in the planes normal to the grain. As the oak wood has approximately $E/G_\perp = 30$, we can estimate that the resonant frequency of the first longitudinal mode is more than five times higher than the resonant frequency of the first torsional mode, and is taken into (29) with a thirty times lower weight. In the other words, the error function (29) is similarly sensitive to an 1% experimental error in the first torsional mode and to a 30% error in the first longitudinal mode. By a particular choice of material (large difference between E and $G_\perp$) and of geometry (1D rod with allowed axially symmetric modes of vibrations) we have disabled a reliable determination of E by any inverse procedure based on minimization of the error function (29).

For generally anisotropic, three-dimensional specimens, the way how the information on the elastic coefficients is distributed in the resonant spectrum is extremely complicated.

Similarly to the above discussed example, the lowest resonant frequencies of such specimen correspond to the *soft modes* and contain the information only about the smallest (which means mostly shear) coefficients or their combinations. By moving in the spectrum upwards, some modes corresponding to the other (i.e. *harder*) coefficients may appear, but the major part could be still related to the soft ones (e.g. the spectrum may contain 2ω, 3ω, etc. frequencies of multiple modes discussed for highly symmetric specimens in the third conclusive remark in the previous section.)

The question is how to determine which coefficients can be accurately determined from such resonant spectrum and which not. On this purpose, let $\alpha_{1,2,\dots,n}$ be the eigenvectors corresponding to measured eigenfrequencies $f^{\text{exp}}_{1,2\dots,n} = \omega^{\text{exp}}_{1,2\dots,n}/2\pi$, and let $C_{k=1,\dots,m}$ be the set of independent elastic coefficients. The derivative of the frequency f^{exp}_p with respect to the constant C_k can be expressed as (using a formula from the perturbation theory, for further details, check [32])

$$\frac{\partial f^{\text{exp}}_p}{\partial C_k} = \frac{\alpha_p^{\text{T}} \frac{\partial \Gamma}{\partial C_k} \alpha_p}{8\pi^2 f^{\text{exp}}_p}, \tag{32}$$

where no summation over p on the right-hand-side is applied. Consequently, the rate of sensitivity of measured spectrum to the k-th elastic coefficient C_k can be taken as a sum of squares of such derivatives over the whole spectrum, i.e.

$$S_k^2 = \sum_{p=1,\dots,n} \left(\frac{\partial f^{\text{exp}}_p}{\partial C_k} \right)^2 = \sum_{p=1,\dots,n} \left(\frac{\alpha_p^{\text{T}} \frac{\partial \Gamma}{\partial C_k} \alpha_p}{8\pi^2 f^{\text{exp}}_p} \right)^2 . \tag{33}$$

Our aim is to evaluate the elastic constants (or their combinations) which are most accurately determined by the inverse procedure. Let us, for simplicity, consider that what we are trying to find are the linear combinations C^*_k, related to the original set of elastic coefficients C_k by linear equations

$$C_k = \Phi_{kl} C^*_l. \tag{34}$$

To evaluate the sensitivity to such combinations, it is necessary to transform (33) into

$$S_l^{*2} = \sum_{p=1,\dots,n} \left(\frac{\partial f^{\text{exp}}_p}{\partial C^*_l} \right)^2 = \sum_{p=1,\dots,n} \left(\Phi_{kl} \frac{\alpha_p^{\text{T}} \frac{\partial \Gamma}{\partial C_k} \alpha_p}{8\pi^2 f^{\text{exp}}_p} \right)^2 = \Phi_{\cdot l} \mathbf{G}^{\text{T}} \mathbf{G} \Phi_{\cdot l}^{\text{T}}. \tag{35}$$

where

$$\Phi_{\cdot j} = (\Phi_{1l}, \Phi_{2l}, \dots \Phi_{nl}) \qquad \text{and} \qquad \mathbf{G} = \begin{pmatrix} \frac{\partial f^{\text{exp}}_1}{\partial C_1} & \cdots & \frac{\partial f^{\text{exp}}_1}{\partial C_m} \\ \vdots & \ddots & \vdots \\ \frac{\partial f^{\text{exp}}_n}{\partial C_1} & \cdots & \frac{\partial f^{\text{exp}}_n}{\partial C_m} \end{pmatrix}. \tag{36}$$

The matrix $\mathbf{G}^{\text{T}}\mathbf{G}$ is symmetric and positive definite, and its eigenvectors can be, thus, chosen to form an orthogonal normalized system. By sorting this eigenvalues in a decreasing order and choosing $\Phi_{\cdot l}$ to be the l-th eigenvector, we obtain linear combinations C^*_l sorted by sensitivity.

Consider now that we are able to construct an inverse procedure reflecting somehow the way how the information on the unknown elastic coefficients is distributed in the spectrum, i.e. a procedure based on a minimization of

$$\Delta(c_{ij}) = \sum_{p=1}^{n} w_p \left(f_p - f_p^{\text{calc.}}(c_{ij})\right)^2, \tag{37}$$

where w_p are weights tuned such that they do not bias the inversion procedure in the way demonstrated by the above discussed example of the 1D oak wood rod. Another problem can than arise in the optimization itself, especially when only rough initial guesses of the elastic coefficients are on disposal. In the first applications of RUS [2], the calculated and experimentally obtained resonances were arranged into sums like (37) by simple ordering, i.e. the first calculated frequency was subtracted from the first experimentally obtained, the second from the second, etc. The effect which such association of frequencies can have on the minimized function can be clearly seen on the following example.

Consider again a cylindrical rod with axially symmetric modes of vibrations allowed. For this time, let the rod be made of polycrystaline copper, with $E = 110$GPa and $G = 63$GPa, which is a quite small difference ($E/G = 1.75$). As the resonances containing the information on the value of E and on the value of G are close to each other, and as we can evaluate these resonance explicitly (higher frequencies are not disturbed by higher numerical errors), we can safely choose $w_p = 1$ for all p. On the left-hand-side of Fig.3, a contour plot of sum (1) in dependence on E and G is shown, evaluated by simply comparing the first fourteen evaluated resonant frequencies with first fourteen obtainable experimentally (but evaluated here for the correct values of G and E). The sum is obviously unsuitable for minimization. Not only that there multiple minima appearing on $\Delta(E, G)$ (without distinguishing between the longitudinal and torsional modes, the values of E and G are fully interchangeable), but the function $\Delta(E, G)$ is far from smooth, which precludes a meaningful use of any gradient search method.

In the right-hand-side of Fig.3, the same (not weighted) sum is plotted with the *mode identification*, i.e. with the knowledge of which resonances are torsional and which are longitudinal involved. After such improvement, the function $\Delta(E, G)$ becomes fully smooth, with one well defined minimum corresponding to correct values of E and G. For the error function (29) weighted by $1/f_p^2$, the contour plots look nearly the same.

The problem of mode identification was successfully solved by Ogi et al. [17], who scanned one of the surfaces of the vibrating specimen by a laser interferometer. From the projection of displacement patterns into that surface, Ogi et al. were able to identify all the observed modes and arrange the resonances in sum (1) in a correct way. Similar approach was later adopted by Landa et. al [12] and extended by automatic identification of modes, where the measured displacements are fitted with the same order of Legendre polynomials, which enables a reliable comparison to the calculated eigemodes.

However, for a generally oriented, three-dimensional anisotropic specimen, the mode association is possible only for relatively accurate initial guesses of the sought elastic coefficients and for known class and orientation of the anisotropy. That is another factor which

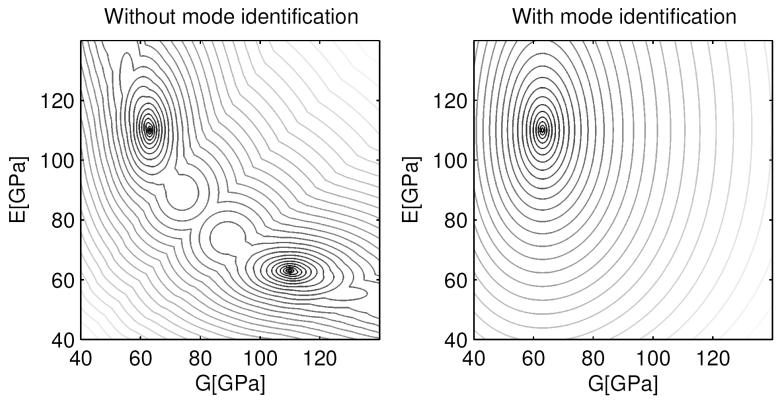

Figure 3: Comparison of the error function $\Delta(E, G)$ without (on the left) and with (on the right) the mode identification.

complicates a general use of RUS and makes it disadvantageous in comparison with pulse-echo measurements: The overall character of the anisotropy can be directly seen neither from the resonant spectra nor from the shapes of the eigenmodes (which mix the symmetry of the material with the symmetry of the specimen), but, without the knowledge of this character, the mode association, and, consequently, the reliable determination of the elastic coefficients can be, in some cases, close to impossible.

Providing that we have tuned the weights such that the sum (37) does not *a priori* suppress the information on any of the sought coefficients and that we have sufficiently accurate initial estimates of the coefficients to identify all the modes involved in the inversion, the inverse procedure could be expected to converge to correct results. The accuracy of these results is given by the experimental error in the input resonant frequencies, by the accuracy of determination of the geometry and orientation of the specimen, by how accurately the frequencies are evaluated within the forward problem (combining the accuracy of the Ritz method with the accuracy of the numerical algorithm used for the solution of the eigenvalue problem (19)), and by the accuracy of the chosen search algorithm (i.e. how accurately the minimum is localized). Such mixing of experimental and numeric errors in the resultant accuracy of the outputs of RUS nearly precludes any direct determination of the accuracy of the method itself. It can be, however, guessed e.g. from Monte-Carlo simulations the input data disturbed randomly within experimentally reasonable ranges, but such approach always enables it to be guessed only for one specific material and one specific geometry of the specimen.

Among the general ways how to increase the accuracy of the RUS measurements, at least the following three points are worth mentioning here:

1. As far as the preparation and choice of the specimens is concerned, it is always better to use the **general bars with mutually undividable dimensions** rather than the

exact cubes or tetragons, **general parallelepipeds** rather than rectangular ones, and **specimens with general orientation** rather than those cut along the principal axes of the specimen. The reason is clear from the discussion of the resonant spectra of highly symmetric specimens (see the previous section). The lower the symmetry of the specimen is (meaning both the shape itself and the specimen's orientation to the symmetry of the material), the more general vibrational modes can be expected to appear. Let it be pointed out here that the modes constructed by multiplication contain exactly the same information on the elastic coefficients as the basic modes they were constructed from. Moreover, for the highly symmetric specimens, some of the modes can be degenerated (i.e. two or more modes can have the same resonant frequency), which significantly complicates the mode identification.

2. The **increase of the degree of the polynomial approximation** (14) can, naturally, increase the accuracy of the obtained results. However, as the dimension of matrix Γ (without any simplification of Γ by possible symmetries considered) is related to the degree of the polynomial approximation by

$$\mathrm{rank}(\Gamma) = \frac{(N+1)(N+2)(N+3)}{2}, \tag{38}$$

each increase of N is penalized by a dramatic increase of computation time. Fig.4 shows comparison of eigenfrequencies computed for three different degrees N: 12, 14 and 16. The dimensions of the matrix Γ were 1365, 2040 and 2907 respectively. The

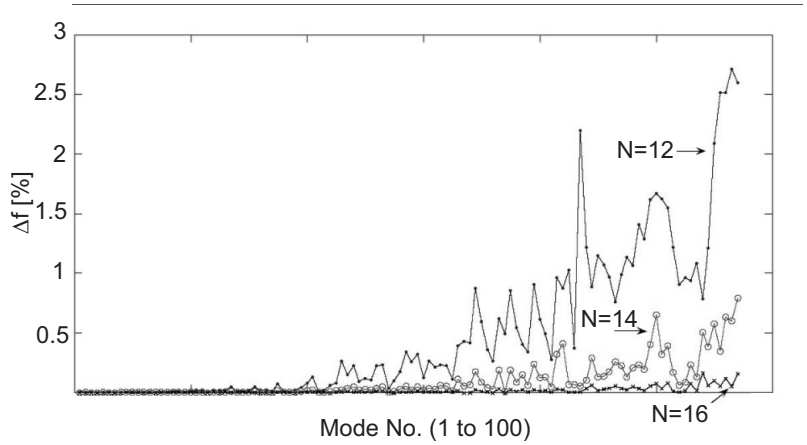

Figure 4: The effect of the degree N of the polynomial approximation on the accuracy of the evaluated resonant frequencies.

solution taken as referential here (i.e. the solution which the resonances calculated for different N are compared to) was obtained by finite element method with very large number of degrees of freedom (10^5). This figure also illustrates another important

feature: Since the plotted quantity here is

$$\Delta f_p = \frac{f_p^{\text{calc.}}(N) - f_p}{f_p}, \tag{39}$$

it can be easily seen that the frequencies for low N are generally higher than both those for higher N and those calculated by finite elements. In other words, the less flexible the approximation is, the more significant shift of the calculated spectrum upwards can be expected.

The choice of the polynomial approximation should also reflect the shape of the specimen, i.e. if the specimen is a thin plate or shell, another (lower) degree of the polynomials should be used to approximate the displacement field distribution along the normals to midplane of the specimen than along the curves inside the midplane.

3. For the search for the optimal coefficients, it is usually beneficial to **decompose the inversion algorithm into particular iterative steps**. The following architecture of inversion procedure was proposed in [32]:

   (a) We consider a parallelepiped sample with given material symmetry, density ρ and shape. Utilizing the 1^{st}-order homogeneity of Γ with respect to the all independent elastic coefficients C_k, we compute the matrices $\partial\Gamma/\partial C_k$ via (21) by setting $C_k = 1$ and $C_j = 0$ for all $j \neq k$.

   (b) We take an initial guess of the constants $C_k^{(0)}$ (e.g. elastic constants of similar materials found in literature), complete the matrix Γ using equations (22), and calculate its eigenvalues and eigenvectors.

   (c) We compute the surface distributions of the displacement field in the surface of the specimen which is scanned by the laser vibrometer. By comparison of computed and experimentally measured distributions, we try to associate measured and computed spectra. If our constants are far from the correct ones (as usually happens for the initial guesses), only the first few modes are associated.

   (d) Using the equations (35) and (36), we compute the matrix $\mathbf{G}^{\mathrm{T}}\mathbf{G}$ with frequencies f_j^{exp} and the eigenvectors α_j^{as} associated to them and determine the linear combinations C_k^* sorted by sensitivity. (The eigenvectors α_j^{as} are not exactly equal to the experimental eigenvectors and thus, the derivatives $\partial f_j^{\text{exp}}/\partial C_k$ used in (35) are approximate only.)

   (e) We minimize the error function

$$\Delta(C_k^*) = \sum_{p_{\text{assoc.}}} \left(f_p^{cal}(C_k^*) - f_p^{exp} \right)^2, \tag{40}$$

   where the summation over $p_{\text{assoc.}}$ means that only the associated modes are taken into account. In [32], (as well as for the results presented in this chapter,) the minimization of (40) is done by a gradient (Levenberg-Marquardt) method,

which provides a fast and straightforward convergence. The efficiency of the inverse determination of the elastic coefficients is improved by deriving the analytical expression of the gradient and the Hessian of the error function using formulae from perturbation theory

$$\frac{\partial \omega_j^2}{\partial C_k^*} = \alpha_j^{\mathrm{T}} \frac{\partial \Gamma}{\partial C_k^*} \alpha_j, \tag{41}$$

$$\frac{\partial^2 \omega_j^2}{\partial C_k^* \partial C_l^*} = \alpha_j^{\mathrm{T}} \frac{\partial \Gamma}{\partial C_k^*} \frac{\partial \alpha_j}{\partial C_l^*} + \left(\frac{\partial \alpha_j}{\partial C_l^*} \right)^{\mathrm{T}} \frac{\partial \Gamma}{\partial C_k^*} \alpha_j, \tag{42}$$

where

$$\frac{\partial \alpha_j}{\partial C_l^*} = \sum_{\substack{i \\ \omega_i \neq \omega_j}} \frac{\alpha_i^{\mathrm{T}} \frac{\partial \Gamma}{\partial C_l^*} \alpha_j}{\omega_j^2 - \omega_i^2} \alpha_i. \tag{43}$$

(f) We estimate the accuracy of evaluated constants C_k^* from the expression

$$\kappa_k = \sqrt{\frac{\sum_{p_{\mathrm{assoc.}}} \left(f_p^{cal} - f_p^{exp} \right)^2}{\sum_{p_{\mathrm{assoc.}}} \left(\frac{\partial f_p^{cal}}{\partial C_k^*} \right)^2}} \approx \frac{\sqrt{\Delta(C_k^*)}}{S_k^*}, \tag{44}$$

where the last approximative equality is exactly satisfied only if $f_p^{\mathrm{cal}} = f_p^{\mathrm{exp}}$ for all associated modes.

The combinations C_k^* with a low value of κ_k (under some chosen threshold) are accepted, the rest is replaced by proper linear combinations of the initial guesses. From such set of C_k^* the original independent coefficients $C_k^{(1)}$ are computed by equations (33). Then, we return to the (b) step of the procedure with new constants $C_k^{(1)}$ and repeat this process until we match all the measured resonance modes and fit their frequencies.

This algorithm using the parameters C_k^* sorted by accuracy κ_k as sought variables (rather than the original constants C_k) enables us to perform the optimization gradually, i.e. to evaluate the most accurately determinable combination C_1^* as the first one (with the rest being fixed), then to evaluate C_1^* and C_2^*, etc., until a chosen sensitivity level is reached. Such inverse procedure is more robust than the classical method optimizing all original constants C_k together [32].

There are, of course, more ways in which the RUS technique can be improved. The accuracy of the input spectra can be improved by taking the attenuation in the material into account, i.e. by considering the effect which the attenuation has on the position of the maxima of the resonance peaks. The experiments can be done in an evacuated chamber to minimize the damping of the specimen by air. However, such particular improvements can slightly correct the obtained results, but undoubtedly cannot help the method to overcome its applicability limits given by material, and exceed, therefor, out of the frame of this chapter.

3 RUS measurements close to applicability limits

Let us now proceed to particular applications of the RUS method for determination of elastic coefficients of various anisotropic solids. The aim here will not be to illustrate the reliability and certainty of RUS when applied to materials for which this method was already verified and provides accurate and easily interpretable results. Quite on the contrary, the issues described in the following text are chosen such that the suitability of the RUS method for their solution is, on the first look, questionable.

In this section, the focus will be laid on the cases where the applicability of RUS is embarrassed due to the properties of the examined material itself. Namely, the particular issues solved within this section will be:

1. the case of **extremely strong anisotropy**, for which the specimen tends to vibrate in the softest modes related to the softest elastic coefficients, and the spectrum, consequently, does not contain sufficient information on the harder ones

2. the case of **weak anisotropy of unknown class of symmetry and unknown orientation**, where the inverse procedure leads to 21-dimensional optimization, as the material must be considered as fully triclinic

3. the case of **temperature dependent attenuation** where the required information (thermal dependencies of elastic coefficients) are shaded by simultaneous changes in the quality of the measured spectrum.

As it was mentioned in the introduction, the modifications of the RUS method described within this chapter cannot be understood as any kind of universal recipes valid for wider classes of similar problems. They are suitable for the particular materials, particular shapes of the specimens and particular experimental arrangements only; they illustrate, according to the main message this chapter aims to bring, the diversity and variability of the world of RUS.

3.1 Extremely strong anisotropy: Single crystals of Cu-Al-Ni

The first example of application of RUS discussed here will be the determination of elastic coefficients of a single crystal of the Cu-Al-Ni shape memory alloy. In the high-temperature *austenitic phase*, the crystal of this alloy has a cubic symmetry. Upon cooling and after applying proper mechanical loading (for details, see [38]), the material can be transformed into the low-temperature *martensitic phase*, which is orthorhombic. The elasticity of the cubic austenite can be fully described by three independent elastic coefficients c_{11}, c_{12} and c_{44}, which are, for the axes set parallel to the principal direction of the material, arranged

in the matrix of elastic coefficients in the following way:

$$c_{ij} = \begin{pmatrix} c_{11} & c_{12} & c_{12} & 0 & 0 & 0 \\ c_{12} & c_{11} & c_{12} & 0 & 0 & 0 \\ c_{12} & c_{12} & c_{11} & 0 & 0 & 0 \\ 0 & 0 & 0 & c_{44} & 0 & 0 \\ 0 & 0 & 0 & 0 & c_{44} & 0 \\ 0 & 0 & 0 & 0 & 0 & c_{44} \end{pmatrix}. \tag{45}$$

After being transformed into martensite, the symmetry of the material decreases into the orthorhombic symmetry. Elasticity of such material can be, then, fully described by nine independent elastic coefficients, which, in natural coordinates of this system, form matrix

$$c_{ij} = \begin{pmatrix} c_{11} & c_{12} & c_{13} & 0 & 0 & 0 \\ c_{12} & c_{22} & c_{23} & 0 & 0 & 0 \\ c_{13} & c_{23} & c_{33} & 0 & 0 & 0 \\ 0 & 0 & 0 & c_{44} & 0 & 0 \\ 0 & 0 & 0 & 0 & c_{55} & 0 \\ 0 & 0 & 0 & 0 & 0 & c_{66} \end{pmatrix}. \tag{46}$$

. The coordinate systems in which the elasticity matrices of austenite and martensite adopt forms (45) and (46) are related by the coordination relations following from the nature of the martensitic phase transition between these two phases (e.g. [39]).

Our aim will be to determine all the independent elastic coefficients of both austenite and martensite from RUS measurements on a single specimen (i.e. the same specimen being first in austenite and then in martensite). The solution of this problem is significantly complicated by the strong anisotropy of the material. In the cubic phase, the strength of the anisotropy can be characterized by the *anisotropy factor*

$$A = \frac{2c_{44}}{c_{11} - c_{12}}. \tag{47}$$

This factor is equal to one for an isotropic material, for common single crystals of metals (aluminium, nickel, copper, gold, silicon) this factor ranges between 0.5 and 5. For the austenitic phase of Cu-Al-Ni, this factor is approximately equal to 12.

What does such high value of A mean physically? To understand it, we have to introduce few fundamental terms of the elastodynamics of anisotropic materials, particularly of the elastic wave propagation. The starting point for us will be the *Christoffel equation* (for derivation, see [40] or any similar textbook)

$$(n_j C_{ijkl} n_l - \rho v_\varphi^2 \delta_{ik}) U_k = 0, \tag{48}$$

which relates the phase velocity of the elastic wave v_φ with the direction of propagation $\mathbf{n}$, the elastic coefficients of the material C_{ijkl}, the density ρ and the polarization vector of the

wave $\mathbf{U}$; δ_{ik} is the Kronecker's symbol. For given direction $\mathbf{n}$, this equation becomes an eigenvalue problem for the so-called *Christoffel matrix*

$$\Gamma_{ik} = n_j C_{ijkl} n_l, \tag{49}$$

which can be solved by finding the roots of secular equation

$$\det(\Gamma_{ik} - \rho v_\varphi^2 \delta_{ik}) = 0. \tag{50}$$

As it follows from definition (49), the Christoffel matrix Γ_{ik} is symmetric and positively definite, therefore its eigenvalues ρv_φ^2 are always real positive and its eigenvectors $\mathbf{U}$ create an orthogonal triplet.

In an isotropic case, the largest eigenvalue $\rho(v_\varphi^{\mathrm{L}})^2$ correspond to an eigenvector $\mathbf{U}^{\mathrm{L}}$ parallel to the direction $\mathbf{n}$, where the superscript L denotes the *longitudintal mode*. The remaining two solutions of (48) coincide in one wave of a *transverse mode* elliptically polarized in plane normal to $\mathbf{n}$, which travels along the direction of $\mathbf{n}$ at phase velocity v_φ^{T}.

In the anisotropic case, the solutions of the Christoffel equation are much more general. The secular equation (50) has, in general, no degenerated roots and the corresponding polarization directions are neither parallel nor normal to the direction $\mathbf{n}$. It is said that the planar waves in each direction can propagate at three different wave modes; one quasi-longitudinal (qL) mode and two quasi-transverse (qT^1, qT^2) modes, withal the qL mode is the one with polarization vector $\mathbf{U}^{\mathrm{qL}}$ closest to the direction of propagation $\mathbf{n}$.

In principal directions of a cubic material, the phase velocities can be expressed analytically. In particular, in the [110] direction of a cubic crystal, the phase velocities are

$$v_\varphi^{\mathrm{qL}} = \sqrt{\frac{c_{11}+c_{12}+2c_{44}}{2\rho}} \stackrel{\text{def}}{=} \sqrt{\frac{c_L}{2\rho}}, \qquad v_\varphi^{\mathrm{qT}^1} = \sqrt{\frac{c_{44}}{\rho}}$$

$$\text{and} \qquad v_\varphi^{\mathrm{qT}^2} = \sqrt{\frac{c_{11}-c_{12}}{\rho}} \stackrel{\text{def}}{=} \sqrt{\frac{c'}{\rho}}. \tag{51}$$

The anisotropy factor A relates, thus, the phase velocities of qT^1 and qT^2 modes in this direction by relation

$$v_\varphi^{\mathrm{qT}^1} = \sqrt{A} v_\varphi^{\mathrm{qT}^2}. \tag{52}$$

So, for A being approximately equal to twelve, we get

$$v_\varphi^{\mathrm{qT}^1} = 2\sqrt{3} v_\varphi^{\mathrm{qT}^2}. \tag{53}$$

Moreover, as the cubic materials typically have[2] $v_\varphi^{\mathrm{qL}} \approx 2 v_\varphi^{\mathrm{qT}^1}$, we can write

$$v_\varphi^{\mathrm{qL}} = 2 v_\varphi^{\mathrm{qT}^1} = 4\sqrt{3} v_\varphi^{\mathrm{qT}^2}. \tag{54}$$

[2] for the [110] direction in the examined single crystal of Cu-Al-Ni, this ratio is even higher, approximately equal to 2.2

In other words, if the specimen of such material was a 1D rod (similar to the oak wood rod considered in the introduction) cut along the [110] direction, the first resonant frequency corresponding to c' would be approximately two times lower than the first one corresponding to c_{44} and nearly seven times lower than the first one corresponding to c_L. With the multiplication of the modes taken into account, we can approximately say that 70% of the spectrum of such rod would contain the information on c' whereas only 10% on c_L. With all the resonant frequencies determined with the same accuracy, we can, thus, expect the coefficient c_L to be obtainable with seven times higher experimental error than c'.

In a real 3D specimen, the information on particular elastic coefficients is in the spectrum distributed even less uniformly, as it is illustrated by the following experimental example. The examined specimen was a parallelepiped of the austenite with dimensions 5.11 x 6.16 x 5.22mm and orientations [0.53; -0.80; -0.26], [0.81; 0.58; -0.07], [0.21; -0.15; 0.96], i.e. with two directions close to [1-10] and [110] principal axes and the third one close to [001]. The RUS measurement was performed in the frequency range 0.1-0.6MHz which resulted in 65 identified modes, which seems to be an inappropriately large number for identification of three independent coefficients. The inverse procedure was run in the multi-stage modification (see the third item of the concluding discussion in subsection 1.3) to obtain an orthogonal set of combinations of elastic coefficients sorted by accuracy. The resulting combinations $C^*_{k=1,2,3}$ are listed in Tab.1. Unsurprisingly, the most accurately determined combination is nearly exactly equivalent to c' and the second one to c_{44}. As the combinations C^*_k are orthogonal by definition, the last combination cannot be equivalent to c_L, but it (similarly to c_L) contains the information on $c_{11} + c_{12}$.

It is obvious that the inaccuracy in C^*_3 is unacceptably high. The resonant spectrum simply does not contain sufficient information on the c_L coefficient, which is related to longitudinal modes of propagation. The applicability of the RUS method is here restricted to accurate determination od coefficients c' and c_{44}. The full anisotropy cannot be captured, unless even more higher modes are taken into account.

Let us, on the other hand, make a short comparison of the RUS method with the pulse-echo measurements, where the elastic coefficients are obtained from values of phase velocities by inverting relations similar to (51). Let us consider a specimen being cut exactly along the [110], [1-10] and [001] directions. In the the [110] and [1-10] directions, the

k	Combination	C^*_k [GPa]	κ_k [GPa]
1	$0.71c_{11} - 0.70c_{12} + 0.07c_{44}$	18.11	0.14
2	$0.01c_{11} + 0.1c_{12} + 0.99c_{44}$	108.38	2.14
3	$0.7c_{11} + 0.71c_{12} - 0.08c_{44}$	169.46	34.94

Table 1: Combinations of elastic coefficients for the austenitic phase of SMA and the accuracies which are the combinations determined with.

velocities are given by (51), in the [001] directions, the relations are

$$v_{\varphi}^{\mathrm{qL}} = \sqrt{\frac{c_{11}}{2\rho}}, \qquad v_{\varphi}^{\mathrm{qT}^1} = v_{\varphi}^{\mathrm{qT}^2} = \sqrt{\frac{c_{44}}{\rho}}. \tag{55}$$

Obviously, the coefficients c_{11} and c_{44} can be conveniently determined from measurements of longitudinal and shear wave phase velocities in direction [001]. Then, it is sufficient to measure the qL velocity in direction [110] to evaluate c_{12} as $2\rho\left(v_{\varphi[110]}^{\mathrm{qL}}\right)^2 - 2c_{44} - c_{11}$. But how does it look like with the accuracy?

Consider that we obtain the phase velocities in forms $v_{\varphi[001]}^{\mathrm{qL}} \pm \delta v_{\varphi[001]}^{\mathrm{qL}}$, $v_{\varphi[001]}^{\mathrm{qT}} \pm \delta v_{\varphi[001]}^{\mathrm{qT}}$ and $v_{\varphi[110]}^{\mathrm{qL}} \pm \delta v_{\varphi[110]}^{\mathrm{qL}}$. Using the known rules for recalculation of experimental errors between quantities, we can write that

$$c_{11} = \rho\left(v_{\varphi[001]}^{\mathrm{qL}}\right)^2 \pm 2\rho v_{\varphi[001]}^{\mathrm{qL}} \delta v_{\varphi[001]}^{\mathrm{qL}}, \tag{56}$$

$$c_{44} = \rho\left(v_{\varphi[001]}^{\mathrm{qT}}\right)^2 \pm 2\rho v_{\varphi[001]}^{\mathrm{qT}} \delta v_{\varphi[001]}^{\mathrm{qT}}, \tag{57}$$

and finally

$$\begin{aligned} c_{12} = {} & \rho\left(v_{\varphi[110]}^{\mathrm{qL}}\right)^2 - 2\rho\left(v_{\varphi[001]}^{\mathrm{qT}}\right)^2 - \rho\left(v_{\varphi[001]}^{\mathrm{qL}}\right)^2 \\ & \pm 2\rho\left(v_{\varphi[110]}^{\mathrm{qL}} \delta v_{\varphi[110]}^{\mathrm{qL}} + 2v_{\varphi[001]}^{\mathrm{qT}} \delta v_{\varphi[001]}^{\mathrm{qT}} + v_{\varphi[001]}^{\mathrm{qL}} \delta v_{\varphi[001]}^{\mathrm{qL}}\right). \end{aligned} \tag{58}$$

For c' evaluated now as $c_{11} - c_{12}$, the experimental accuracy is

$$\delta c' = \rho\left(v_{\varphi[110]}^{\mathrm{qL}} \delta v_{\varphi[110]}^{\mathrm{qL}} + 2v_{\varphi[001]}^{\mathrm{qT}} \delta v_{\varphi[001]}^{\mathrm{qT}} + 2v_{\varphi[001]}^{\mathrm{qL}} \delta v_{\varphi[001]}^{\mathrm{qL}}\right). \tag{59}$$

If we take into account that

$$v_{\varphi[110]}^{\mathrm{qL}} \approx \sqrt{2} v_{\varphi[001]}^{\mathrm{qL}} \approx 2v_{\varphi[001]}^{\mathrm{qT}} \tag{60}$$

and consider that all the phase velocities were determined with the same accuracy, i.e. that

$$\delta v_{\varphi[110]}^{\mathrm{qL}} \approx \delta v_{\varphi[001]}^{\mathrm{qL}} \approx \delta v_{\varphi[001]}^{\mathrm{qT}}, \tag{61}$$

we can conclude that c' is from the pulse-echo measurements determined with $(4 + 2\sqrt{2})$ times lower accuracy than c_{44}. As c' is approximately five times smaller than c_{44}, the pulse echo measurements at the level of 1% experimental error in c_{44} results in nearly 35% error in determination of c'.

If the coefficient c' is not determined from the above procedure but from direct measurements of the $v_{\varphi[110]}^{\mathrm{qT}^2}$ velocity, the accuracy can be incomparably higher. However, the experimental determination of this velocity is extremely complicated. In paper [38], the authors examined variously oriented single crystals of Cu-Al-Ni by pulse echo methods, but were not able to detect reliably this wave in any direction. Similarly, Stipcich et al. [41]

k	Dominating terms	C_k^* [GPa]	κ_k [GPa]
1	$c_{11}+c_{22}+2c_{55}-2c_{12}$	51.93	0.37
2	$-c_{11}-c_{22}+2c_{55}+c_{12}$	18.34	0.90
3	$2c_{44}+2c_{66}$	115.92	2.77
4	$2c_{44}-2c_{66}-c_{23}$	10.98	3.56
5	$2c_{33}-c_{23}-2c_{13}$	8.02	5.75
6	$c_{11}+c_{44}+2c_{23}-c_{13}-c_{12}$	25.63	5.87
7	$2c_{11}-2c_{22}+c_{33}-c_{23}+c_{13}$	111.60	17.08
8	$2c_{11}+c_{22}-1c_{33}+2c_{12}$	182.55	53.35
9	$c_{22}+2c_{33}+c_{23}+c_{13}$	302.09	73.54

Table 2: Combinations (dominating terms only) of elastic coefficients of martensite of Cu-Al-Ni sorted by accuracy they can be determined with.

were not able to detect any reliable echo for this velocity in Ni-Mn-Ga although their specimen was cut exactly along the (110) planes. On the other hand, this wave was repeatedly measured in materials with lower anisotropy factors, such as Co-Al-Ni ([42], A =4) or Cu-Al-Mn ([43], A =5.4). The reasons are numerous (e.g. strong magneto-elastic attenuation as discussed in subsection 3.3), but the most important of them probably is that for such strong anisotropy, the qT^2 mode is extremely strongly affected by the *directional dispersion*, i.e. by the fact that the anisotropy focuses the energy carried by qT^2-waves to few preferred directions whereas the others (e.g. the [110] direction) become energetically suppressed (more details on this effect can be found, again, in [40] or any similar textbook).

For c' determined as the difference between experimentally obtained c_{11} and c_{12}, the experimental error of this coefficient (59) is similarly unacceptable as the error in C_3^* obtained from RUS measurements. This lead us to the idea, that the RUS and pulse-echo measurements can be, in some sense, complementary to each other, and that their combination could be a good way how to determine the elastic coefficients of strongly anisotropic materials. This idea will become essential in the second part of this subsection, where we will try to determine the elastic properties of the same specimen but after being transformed into a single variant of martensite.

In the monovariant of martensite, the shape of the specimen was a non-rectangular parallelepiped (5.14mm$\times$5.92mm$\times$5.39mm) with face normals [-0.71; 0.58; -0.37], [0.32; 0.84; 0.42], [0.55; 0.23; -0.80] in the natural coordinate system of the orthorhombic crystal lattice of martensite. RUS measurement was performed in the frequency range 0.1-0.8MHz, 70 resonances were involved in the inversion procedure, which was, again, run in the multi-stage modification with the result obtained in a form of orthogonal combinations of elastic coefficients sorted by accuracy. These results are outlined in Tab.2, where the combinations are reduced to few dominating terms to highlight the particular character of each of them. Obviously, the combinations Nos.7$\div$9 are extremely inaccurately determined. The question is, whether especially these three combinations can be determined by pulse-echo measure-

ments, i.e. whether the RUS and pulse-echo measurements are really complementary to each other. As the specimen in martensite has a quite general crystallographic orientation and the class of symmetry is quite low (orthorhombic), no analytic formulae can be derived to relate the phase velocities in the direction normal to the parallelepiped's faces with the elastic coefficients. These relations must me sought numerically, namely by analyzing which of the combinations from Tab.2 depend sensitively on values of which phase velocities. On this purpose, the partial derivatives of particular phase velocities with respect to the combinations $\partial v_\varphi / \partial C_k^*$ were approximated by finite differences

$$\frac{\partial v_\varphi}{\partial C_k^*} \approx \frac{v_\varphi(C_1^*, \ldots, C_k^* + \delta C_k^*, \ldots, C_9^*) - v_\varphi(C_1^*, \ldots, C_k^*, \ldots, C_9^*)}{\delta C_k^*}, \tag{62}$$

and these differences were evaluated for all modes of propagation (qL, qT^1, qT^2) and three possible directions (normals to the parallelepiped's faces). The result is graphically embodied in Fig.5, from which one can conclude that the relation between the determined combinations and the phase velocities measurable by pulse-echo methods is rather nontrivial. What is undisputable is the fact that the first (the most accurately determined) combination

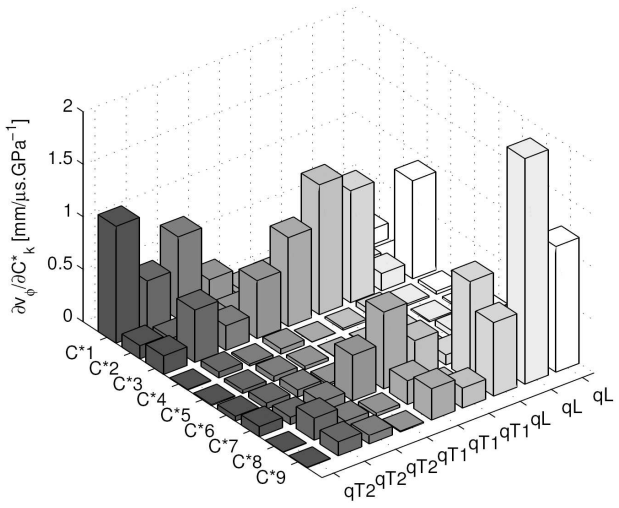

Figure 5: Sensitivity of values of the phase velocities to the combinations of elastic coefficients C_k^*. Labels qL, qT1 and qT2 denote the modes of propagation. For each mode, three velocities are considered, corresponding to three directions given by the normals to the specimen's faces.

C_1^* is somehow related to the qT^2 mode of propagation whereas the last (the least accurately determined) combination C_9^* to the qL mode. This is an evident similarity with the previous case of the austenitic specimen. On the other hand, the combinations cannot be strictly divided by their correspondence to particular modes of propagation, as the combination No.3 is sensitively dependent to all modes of propagation. On the other hand, the

Source	c_{11} [GPa]	c_{22} [GPa]	c_{33} [GPa]	c_{44} [GPa]	c_{55} [GPa]	c_{66} [GPa]	c_{23} [GPa]	c_{13} [GPa]	c_{12} [GPa]
RUS	187.17 $\pm$16.47	149.18 $\pm$15.00	236.38 $\pm$27.10	69.40 $\pm$2.96	22.62 $\pm$0.82	63.01 $\pm$3.85	93.07 $\pm$16.43	65.03 $\pm$17.77	140.18 $\pm$14.77
RUS & qL	185.38 $\pm$1.83	147.55 $\pm$1.87	229.89 $\pm$0.84	71.02 $\pm$1.85	22.93 $\pm$0.53	63.74 $\pm$1.69	97.35 $\pm$2.14	74.11 $\pm$1.51	138.96 $\pm$1.01
[38]	184.46 $\pm$1.12	151.45 $\pm$0.75	238.58 $\pm$1.87	66.39 $\pm$0.21	22.85 $\pm$0.18	60.55 $\pm$0.40	86.83 $\pm$1.05	70.09 $\pm$1.07	140.41 $\pm$0.77

Table 3: Elastic coefficients of the martensitic phase of Cu-Al-Ni. The results obtained by RUS and by combination of RUS and pulse-echo measurements of qL velocities is compared to the results of [38] obtained by pulse-echo measurements on various specimens.

combinations Nos.4÷6 do not significantly correspond to any of the modes of propagation. The question is how the above findings can improve the inverse evaluation of the elastic coefficients. The quasi-longitudinal velocities v_φ can be easily measured using the pulse-echo technique, so this additional information may be used for more accurate determination of combinations Nos.7÷9. The most natural approach seems to be the direct involvement of the phase velocities into the optimizing process, i.e. adding a term

$$\Delta_\varphi = \sum_{n=1}^{3} (v_\varphi^{\text{cal}}(C_{ijkl}) - v_\varphi^{\text{exp}})^2 \tag{63}$$

to the error function (1). However, such extension of the error function disables the construction of linear combinations, and the whole optimization process becomes more complicated. Another possibility is to take the combinations No.1÷6 as precisely determined from the RUS measurements, and Nos. 7÷9. as independent. After the combinations Nos.1÷6 are determined from the frequency spectrum, the remaining combinations can be easily fitted to the longitudinal phase velocities. This approach enables us to reach the average difference between measured and calculated qL phase velocities to be smaller than 10^{-6}mm/μs without disturbing the optimality of the fit between the measured and calculated spectra. Tab.3 compares the accuracies of individual independent coefficients evaluated without and with involving the qL phase velocities in the algorithm. In the first row, the estimates of the experimental errors were obtained from κ_k by the linear relation

$$\delta C_k = |\Phi_{kl}| \frac{\kappa_l}{3}, \tag{64}$$

where Φ_{kl} are the coefficients of the combinations (34) and the factor $\frac{1}{3}$ reflects the fact that the $[C_k^* - \kappa_k; C_k^* + \kappa_k]$ is assumed as a 3σ-interval. In the second row, a similar procedure was applied, but with the 3σ intervals of combinations Nos.7÷9 determined by Monte Carlo simulation with the requirement of agreement in qL phase velocities being better than 10^{-6}mm/μs. The impact of involvement of the qL phase velocities into the inverse algorithm is dramatic: The experimental errors in coefficients c_{33}, c_{13}, and c_{12} are reduced more ten times. The smallest improvement is in the coefficients c_{44}, c_{55} and c_{66},

i.e. in the shear coefficients closely related to the first (softest) eigenmodes and already accurately determined by RUS.

In Tab.3 the results from RUS are also compared to these obtained from pulse-echo in fifteen different directions (see [38] for more detail). The accuracies of the coefficients from [38] seem to be slightly higher (except of c_{33}). However, they were obtained by Monte Carlo simulations with chosen input errors in the values of phase velocities and in the specimen orientation, and are, thus, artificial in some sense; the experimental errors of the results of RUS were, on contrary, evaluated directly from the nature of the method by definition (44). Moreover, it must be pointed out that the results from RUS were obtained on one specimen only, whereas in [38], five differently oriented specimens were used.

In general, we can conclude that the RUS method can be applied to materials with extremely strong anisotropy, but the results cannot be expected to have satisfactory accuracy unless some additional information is involved, e.g. the values of qL phase velocities in given directions of the material. For the cubic austenite, the RUS method and the inversion from phase velocities are fully complementary – the first cannot accurately determine the c_L coefficient, the latter the c' coefficient. In the case of the orthorhombic martensitic phase, the situation is more complicated, but the combination of RUS and pulse-echo measurements can result in acceptably accurate determination of all independent elastic coefficients.

3.2 Weak (averaged) anisotropy: Elastic properties of finely grained materials processed by ECAP

Consider now a quite different problem. Let the specimen be a parallelepiped again, but not a single crystal, where the orientations can be accurately determined from X-ray measurements, but a *textured polycrystal*, where the anisotropy has a statistical, averaged character which can be given by both the preferred crystallographic orientation of the grains and the microstructure (i.e. the pattern of grain boundaries). In such case, the principal axes of the symmetry (if there are any) are completely unknown, as well as the class of the symmetry[3]. To characterize the elasticity of the material, a full triclinic description with 21 independent elastic coefficients must be used in the first step; the character and orientation of the anisotropy can be only estimated *a posteriori* by finding some cartesian system in which the tensor C_{ijkl} has the highest symmetry. The only reasonable assumption we can do about such anisotropy is that to expect it to be weak, i.e. to be describable as a small perturbation of the isotropic elasticity of an untextured polycrystal with isotropic microstructure. Obviously, the RUS technique is unreplaceable here, since the information obtainable from pulse-echo measurements (three triples of phase velocities in directions normal to the faces of the specimen) can never be sufficient for determination of all 21 constants. Let it be pointed out that this problem is completely different from the case discussed by Sarrao et

[3]Both the class and the orientation of the anisotropy can be sometimes approximately guessed from optical or EBSD microscopy of the grain texture, but as our primary aim is to check the power of the RUS method to solve this problem, we will not take any such additional information into account.

k	Dominant coefficients	C_k^* [GPa]	κ_k [GPa]
1.	$c_{11}+c_{22}+c_{33}+2c_{44}+2c_{55}+2c_{66}-c_{23}-c_{13}-c_{12}$	119.47	0.18
2.	$c_{33}+c_{44}+2c_{55}-3c_{66}-c_{13}-c_{46}+c_{56}$	23.29	0.32
⋮	⋮	⋮	⋮
16.	$c_{22}+c_{33}-c_{13}-2c_{25}+2c_{35}+c_{24}-c_{26}-c_{34}+c_{36}+c_{45}$	22.06	7.30
17.	$-c_{22}+c_{33}-c_{44}-c_{23}+c_{13}-c_{12}+c_{25}-c_{35}+2c_{14}+2c_{24}-2c_{34}$	45.48	9.64
18.	$c_{11}+2c_{33}+c_{23}+c_{13}-c_{14}-c_{16}-c_{24}-c_{26}-c_{34}-2c_{36}$	1.83	22.15
19.	$c_{22}+c_{12}+c_{14}-c_{16}+2c_{24}-c_{26}+2c_{34}-c_{36}$	183.06	40.20
20.	$c_{11}+c_{22}+c_{33}+c_{13}+c_{12}+c_{15}+c_{25}+c_{35}$ $+c_{46}+c_{14}+c_{16}+c_{24}+c_{26}+c_{34}+c_{36}$	70.10	49.41
21.	$c_{11}+c_{22}+c_{13}+c_{12}-2c_{15}-2c_{25}-2c_{35}+c_{14}+c_{24}+c_{36}$	182.14	58.83

Table 4: Combinations of elastic coefficients (dominating terms only) for a weakly anisotropic, nanograined polycrystal of copper sorted by accuracy.

al. [16], who have shown that the RUS method can be suitable for determination of crystallographic orientations of small single crystals. The main difference is that Sarrao et al. knew *a priori* the class of symmetry of the examined material, which enabled them to extend the inverse procedure by involving the orientation of the principal axes as additional sought unknown variables.

As an illustrative example, we will evaluate the elastic properties of a polycrystal of copper processed by *equal channel angular pressing* (ECAP) [44–47]. ECAP technology is a method for manufacturing of fully dense nanoscopically grained materials, based on subjecting the material to repeated plastic deformation by moving a workpiece several times through a die containing two intersecting channels of identical cross-sections. During each processing cycle, the grains become finer. The first pass of the workpiece induces the pattern in grain boundaries, which rotates for a small angle during every pass.

The specimen used in our experiments was a $3\times5\times7$mm rectangular parallelepiped, cut from the workpiece after the first route through the processing die. The one pass only was chosen because the material in this state has the weakest anisotropy – the microstructure of the grain boundaries does not play such important role as after many passes where the grains are much smaller (and the volume fraction of the grain boundaries, thus, much higher). The density of the specimen was expected to be the same as for common polycrystalline copper (8.96 g.cm^{-1}). This specimen was investigated by the common RUS procedure, taking first 100 resonances and the shapes of corresponding eigenmodes as an input. Similarly as for the previous case of extremely strong anisotropy, the multi-stage inverse algorithm was applied, and thus, the result was obtained in a form of linear combinations of the sought elastic coefficients sorted by accuracy. As the initial guesses, isotropic elastic coefficients of polycrystalline copper were taken. These guesses enabled reliable identification most of the input modes.

Tab.4 includes the first (i.e. the most accurately determined) two and the last (i.e. the

least accurately determined) six combinations. In this table, not the full combinations are listed (each having 21 terms) but only few dominating terms are shown to highlight the overall character of each combination. Obviously, the first of these combinations has a strong physical meaning. As our material is nearly isotropic, we can consider for a while that

$$c_{11} \approx c_{22} \approx c_{33}, \tag{65}$$

$$c_{12} \approx c_{23} \approx c_{13}, \tag{66}$$

$$\text{and } c_{44} \approx c_{55} \approx c_{66} \approx \frac{c_{11}-c_{12}}{2}. \tag{67}$$

Then, the combination No.1 is proportional to c_{44}, which is the the shear modulus of the isotropic continuum.

The relation between the first combination and the shear velocities is clear even when a full anisotropy is considered. Being written in form

$$C_1^* \sim c_{44}+c_{55}+c_{66}+\frac{c_{11}-c_{12}}{2}+\frac{c_{22}-c_{23}}{2}+\frac{c_{33}-c_{13}}{2}, \tag{68}$$

this combination can be approximately understood as an average value of squares of shear velocities in various principal directions. Similar discussion can be done also for the second combination, where, for the isotropic continuum ($c_{46} \approx c_{56} \approx 0$), the dependence remains on c_{44}, c_{55}, c_{66} and $\frac{c_{33}-c_{13}}{2}$ only, which are all equal to the shear modulus again.

The last four combinations (Nos. 18÷21) are extremely inaccurately determined. For this reason we decided to tune these combinations by pulse-echo measurement in a similar way as it was done in the previous subsection for the strong anisotropy. Seven phase velocities (three quasilongitudinal and four quasitransverse) were taken into account. After such correction, the resultant triclinic elasticity with coefficients

$$c_{ij} =$$

$$= \begin{pmatrix} 199.70 \pm 0.79 & 111.50 \pm 0.92 & 102.65 \pm 0.80 & 5.39 \pm 1.54 & 4.64 \pm 1.09 & -0.68 \pm 0.76 \\ & 196.87 \pm 1.10 & 109.08 \pm 0.67 & 6.33 \pm 1.45 & 3.40 \pm 1.54 & -1.85 \pm 0.62 \\ & & 200.83 \pm 1.46 & 5.53 \pm 1.39 & 2.06 \pm 1.43 & -3.90 \pm 1.20 \\ & & & 42.29 \pm 0.42 & 1.69 \pm 0.95 & 0.19 \pm 0.87 \\ & \text{symm.} & & & 42.65 \pm 0.42 & 0.01 \pm 0.55 \\ & & & & & 42.62 \pm 0.42 \end{pmatrix} \text{GPa} \tag{69}$$

approximated all these phase velocities with errors lower than 0.05mm.μs^{-1}. Similarly as in the case of the martensite of the Cu-Al-Ni, the estimates of experimental errors were recalculated from the known linear relations between C_k^* and c_{ij}

Let us now try to identify the class and orientation of the anisotropy to lower the number of independent coefficients to the essential minimum. As the material is nearly isotropic, the surfaces of the phase velocity (qL, qT^1, qT^2) are close to spheres. On contrary, the difference between the quasishear velocity surfaces qT^1−qT^2 (which is identically equal to

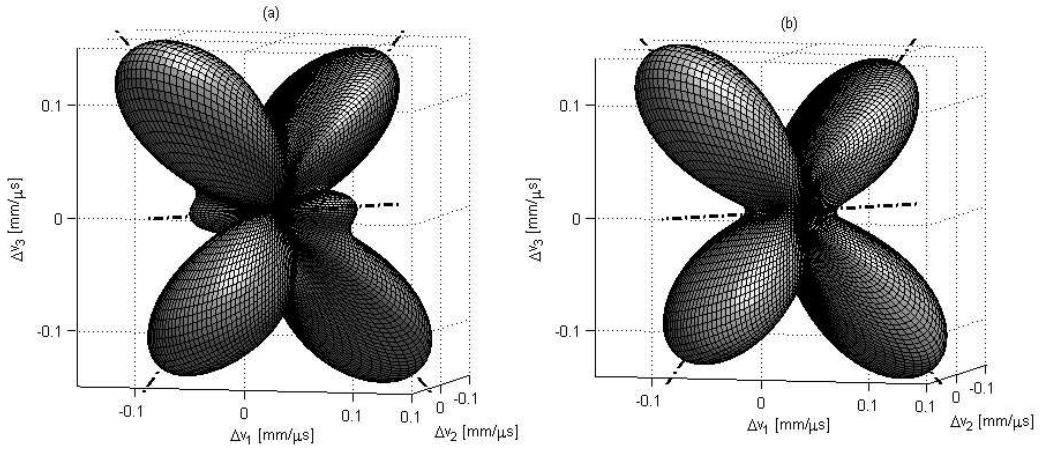

Figure 6: Surfaces of difference between qT velocities: (a) fully triclinic anisotropy determined by RUS method in combination with pulse-echo measurements of qL phase velocities; (b) orthorhombic approximation of the material.

zero in the isotropic material) copies sensitively the symmetry of the material, and can be, thus, used for its identification.

In Fig.6(a), the surface of the difference

$$\Delta v(\mathbf{n}) = v^{\mathrm{qT}^1}(\mathbf{n}) - v^{\mathrm{qT}^2}(\mathbf{n}) \tag{70}$$

is plotted in the axes given by the edges of the specimen. Obviously, this surface has higher class of symmetry than fully triclinic. Three mutually orthogonal axes can be easily identified, having a general orientation to the edges of the specimen. After rotating the matrix (69) onto these orthogonal axes and setting the coefficients

$$c_{14} = c_{15} = c_{16} = c_{24} = c_{25} = c_{26} = c_{34} = c_{35} = c_{36} = c_{45} = c_{46} = c_{56} = 0, \tag{71}$$

we obtain an orthorhombic system with the elastic coefficients (in the rotated axes)

$$c_{ij} =$$

$$= \begin{pmatrix} 203.74 \pm 1.64 & 106.23 \pm 0.67 & 116.79 \pm 1.63 & 0 & 0 & 0 \\ 106.23 & 182.97 \pm 1.35 & 105.64 \pm 0.90 & 0 & 0 & 0 \\ 116.79 & 105.64 & 199.82 \pm 0.29 & 0 & 0 & 0 \\ & & & 41.26 \pm 0.40 & 0 & 0 \\ & \text{symm.} & & & 42.31 \pm 0.26 & 0 \\ & & & & & 49.42 \pm 0.17 \end{pmatrix} \text{GPa}, \tag{72}$$

where the experimental errors were determined by simply rotating the matrix of accuracies from (69) into the coordinates of the orthorhombic symmetry. The $\Delta v(\mathbf{n})$ surface for this system is plotted in Fig.6(b). Fig.7 shows how accurately this orthorhombic system

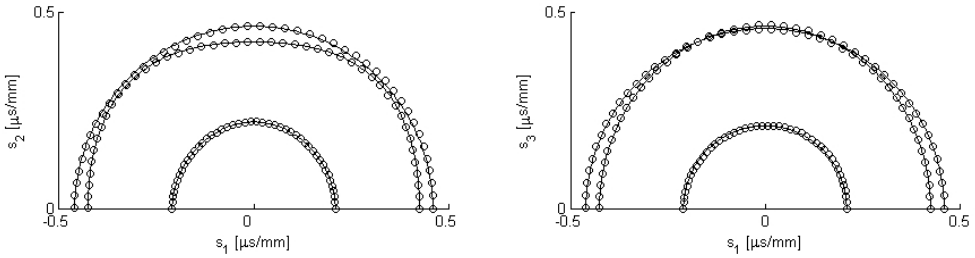

Figure 7: Principal cuts (by x_1x_2 and x_1x_3 planes) of slowness surfaces for the examined material. The circles correspond to fully triclinic anisotropy determined by RUS method in combination with pulse-echo measurements of qL phase velocities, the solid lines to the orthorhombic approximation of the material.

approximates the properties of the original triclinic system. The compared quantities here are the *slowness vector components*, i.e. the reciprocals of the phase velocities. Similarly good agreement can be seen between the resonant spectra and the shapes of the corresponding eigenmodes for the originally considered full triclinic anisotropy and the identified orthorhombic system. In Fig.8, such comparison is shown. Only for few modes (e.g. mode No.30 in Fig.8) some difference between the shapes of modes evaluated for the triclinic and the orthorhombic symmetry can be seen. The values of resonances are, however, matched with an excellent agreement.

We can conclude that the RUS method (in combination with pulse-echo measurements) is able to identify the class and orientation of anisotropy in weakly anisotropic materials. However, the above outlined procedure can be applied only for nearly isotropic materials, where the isotropy can be used as the initial guess for the inverse algorithm, which enables the mode association.

There is one more remark to be done here concerning the RUS investigation of weak averaged anisotropies, i.e. anisotropies induced not by the crystal lattice but by an oriented microstructure. In the above investigated case of polycrystalline copper processed by ECAP, the texture is nanoscopic, which means that all its characteristic dimensions can be considered as incomparably smaller than the dimensions of the specimen as well as than the wavelengths of the all modes involved in the inverse procedure. However, it is important to understand what the expression *incomparably smaller* exactly means, i.e. how coarse microstructuring will not limit the applicability of RUS.

For simplicity, let us return to our well-tried example of a 1D specimen. The following numerical example gives an illustration of how the coarsening of the microstructure can significantly affect the measurements: A one-dimensional string of 7.2mm in length was considered, consisting of 48, 24, and 12 elements of unit mass density and alternating bending wave velocities $v_\varphi^A = 1\text{mm}/\mu\text{s}$ and $v_\varphi^B = 3\text{mm}/\mu\text{s}$. The volume fraction of the component B was chosen as $\mu = 2/3$. The eigenfrequencies of bending modes of such spring were determined using the COMSOL Multiphysics$^{\text{TM}}$ eigenvalue solver with the

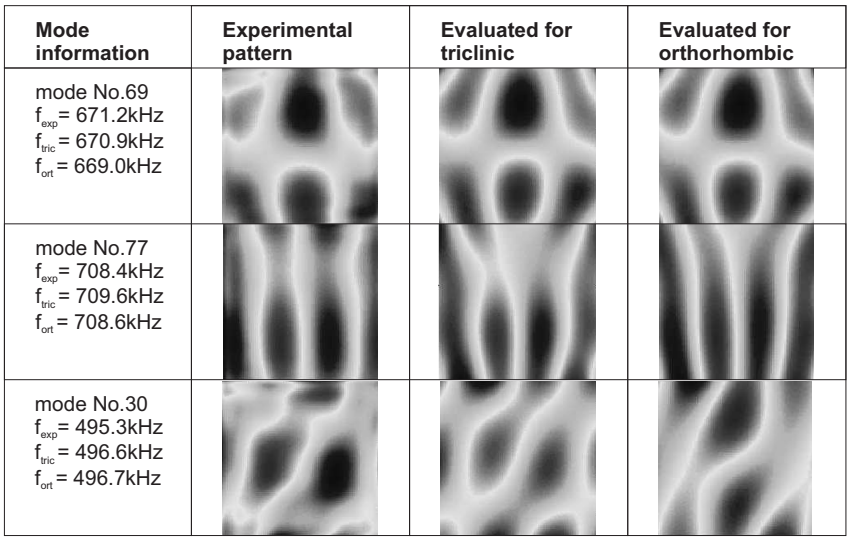

Figure 8: Examples of comparison between measured and evaluated displacement patterns for particular eigenmodes; f_{exp} denotes the experimentally determined eigenfrequency, f_{tric} the corresponding frequency evaluated for the full triclinic matrix (69), f_{ort} for the orthorhombic approximation (72).

spring meshed by 1152 Lagrangian-quadratic finite elements. The stability of the solution was checked by decreasing the FEM mesh density down to 288 elements on the string. The results are shown in Fig.9. For a homogeneous spring, the spectrum should linearly

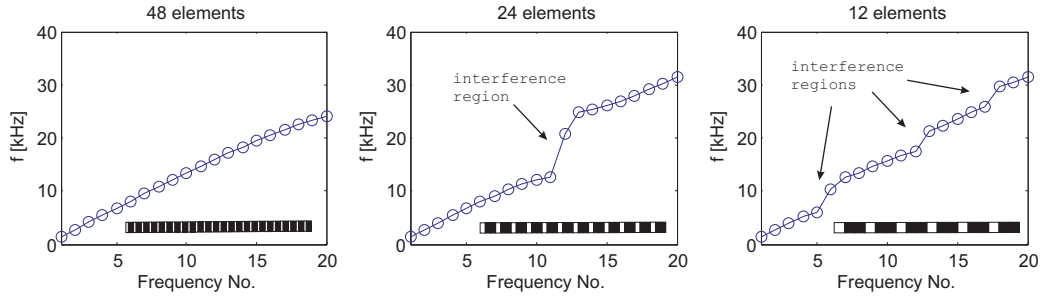

Figure 9: Effect of texture coarsening on eigenfrequencies for a 1D string composed of decreasing number of elements.

increase, as the equation of the steady waves (11) here has form

$$\rho\omega^2 u + S_{A+B}\frac{\mathrm{d}^2 u}{\mathrm{d}x^2} = 0, \tag{73}$$

where S_{A+B} is a bending stiffness obtained by homogenization of the bending properties

of elements of material A and B. However, the results of the numeric simulation show something quite different. Even for the spring consisting of 48 elements, the evaluated spectrum deviates from a linear trend (but remains, for the displayed first 20 eigenfrequencies, increasing smoothly). For 24 elements, a significant jump in a spectrum appears at about 15kHz. Further coarsening (to 12 elements) reveals that such jumps form a periodic serration on the increase of the spectrum, appearing in the regions where the eigenmodes and the structure interfere. We can conclude that even for the ratio between the dimension of the specimen and the characteristic length of the microstructure being equal to 50, the application of RUS for the determination of homogenized (averaged) elastic coefficients may be questionable.

In the more general 3D case, where the eigenmodes, even if they have eigenfrequencies close to each other, may geometrically differ in such way that one of them strongly interferes with the microstructure and the second in not influenced at all, the effect of coarsening on the resultant frequency spectrum becomes more complex. In [49], the effect of the interference between the eigenmodes of vibrations and the microstructure is illustrated for martensitic microstructures of Cu-Al-Ni, i.e. for geometrically ordered mixtures of variously oriented single variants of martensite analyzed in the previous section. For evaluation of the homogenized elastic coefficients of such ordered mixtures, an energetic algorithm described in [48] is used. The conclusion in [49] is that as soon as the thicknesses of particular laminas in the microstructure start to be higher than 100μm, the resonant spectra of a parallelepiped having few millimeters in each dimension exhibit similar interference effects as the above discussed 1D spring.

3.3 Thermal dependencies of elastic coefficients in media with strong magneto-acoustic attenuation: Single crystal of Ni-Mn-Ga

Whereas the above two discussed applications of RUS were rather illustrative (chosen to have extremely strong or extremely weak anisotropy), which enabled their findings to be formulated in clear conclusions, the last case described within this section will concern an application of this method to an extremely complex material, coupling more physical phenomena together. The main aim here will be to show how the RUS applicability can be limited by ultrasound attenuation in the material. However, the findings from the first two subsections will be also utilized.

The internal friction in materials and resulting ultrasound attenuation belong among the most natural limiting factors for RUS measurements. Although the theoretical works dedicated to how the effect of attenuation can be avoided ([36] and the list of references therein) or even exploited for determination of damping parameters [26] are numerous, the essential question is always the same: How to identify the individual resonance peaks within the attenuated spectrum?

Consider now a part of a spectrum containing N resonant frequencies. For f_n being the resonant frequency of the $n-$th mode (n between 1 and N) with amplitude A_n and phase

ϕ_n, the amplitude of a spectrum can be approximated by function

$$F(f_n, A_n, \phi_n, \mathrm{FWHM}_n) = \sum_{n=1}^{N} \frac{A_n \frac{\mathrm{FWHM}_n}{2} e^{\mathrm{i}\phi_n}}{\mathrm{i}(f - f_n) + \frac{\mathrm{FWHM}_n}{2}}, \tag{74}$$

where FWHM_n means *full width at half maximum* of the $n-$th mode, which is one of the possible parameters to measure the attenuation. In Fig.10, the ways how the spectrum can be biased by an increase of FWHM parameters are shown on illustrative synthetic spectra (FWHM here is considered as the same for all plotted peaks). The left–hand–side of the figure shows how a peak of lower amplitude can get completely overlapped by a near peak of higher amplitude. On the right, a junction of two peaks located close to each other is shown, providing that the amplitudes of the peaks are comparable. Obviously, it is nearly impossible to decompose the attenuated spectrum into individual peaks without at least an approximative knowledge about the number and the locations of the resonant frequencies contained in it.

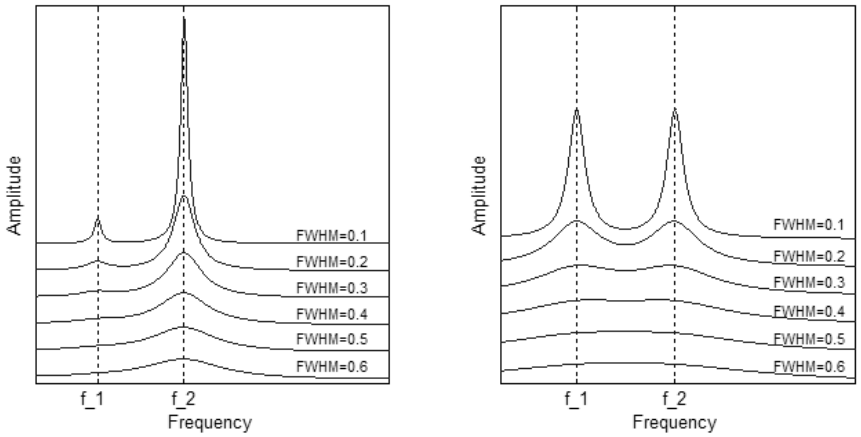

Figure 10: The effect of increasing attenuation on the spectrum: Disappearance of smaller peaks (on the left) and junction of neighboring peaks with comparable amplitudes (on the right).

In the following example, the attenuation combines with an extremely strong cubic anisotropy (comparable to that investigated in section 3.1), which makes the application of RUS even more complicated. On the other hand, the findings from the section 3.1 will be shown as very helpful in this case, and will enable us to determine quite accurately the c' coefficient, although only few peaks from the spectrum will be identified. The examined specimen is a $7.7\times5.6\times4.4$mm rectangular parallelepiped (cut approximately along the principal $\{100\}$ planes) of a near stoichiometric Ni-Mn-Ga alloy, which exhibits extremely strong magneto-elastic attenuation in the temperature interval between the premartensitic transition temperature ($T_{\mathrm{pM}} \approx 257$K) and the Curie point ($T_{\mathrm{C}} \approx 385$K). In [50], this attenuation

has been investigated by combination of ultrasonic methods (pulse–echo measurements of longitudinal waves in [100] and [110] directions and the RUS). The results have shown that this attenuation is strongly anisotropic (see Fig.11 for an outline):

- The attenuation of longitudinal waves in the [100] direction is completely unaffected by the T_{pM} temperature. It increases towards some maximal attenuation, and then it falls down till the Curie point is reached, where it changes significantly its slope.
- The attenuation of longitudinal waves in the [110] direction jumps discontinuously at the T_{pM} temperature and increases steeply to the maximum (which is at slightly higher temperature than for the [100] direction). With further increase of the temperature, the attenuation slowly decreases, but seems to be fully unaffected by the T_{C} temperature.
- The attenuation of the first mode detected within the spectrum obtained by RUS measurements exhibits a significant change of the slope at T_{C} and steeply increases with further decrease of the temperature. However, at about $T = 280$K, further measurements (in the fully non-contact regime) were disabled by water vapor condensation at the faces of the specimen.

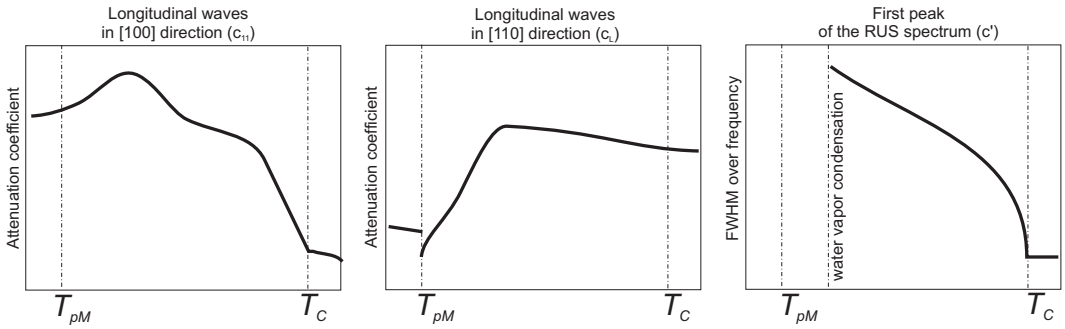

Figure 11: Anisotropic character of the attenuation in the Ni-Mn-Ga single crystal; sketched after the results of [50].

Here, we will focus on the RUS measurements only. The effect which the magnetoelastic attenuation has on the spectrum is illustrated by Fig.12, where the spectra in frequency band 50–170kHz are plotted for three different temperatures: Above the Curie point (i.e. at 389K), the spectrum has a good quality and all the resonant frequencies can be reliably determined. Below the Curie point (353K), the quality of the spectrum significantly decreases. Individual peaks start overlapping and merging. This effect is even more evident at 317K, where the spectrum is such strongly attenuated that the identification of individual resonances with acceptable accuracy is close to impossible. Another effect illustrated by Fig.12 is the drift of the whole spectrum with the temperature. Upon cooling, the first resonant frequency moves from 76.1kHz above the Curie point down to 60.1kHz at 317K. The rest of the spectrum (or at least the part of the spectrum shown in Fig.12) drifts in a similar

way. Such dramatic changes of the resonances with the temperature cannot be ascribed to the thermal expansion of the specimen, which is about 18.10^{-6}m.K^{-1} [51] (which means that the shifts in the resonances should be also at about 10^{-5} level). The resonant spectra

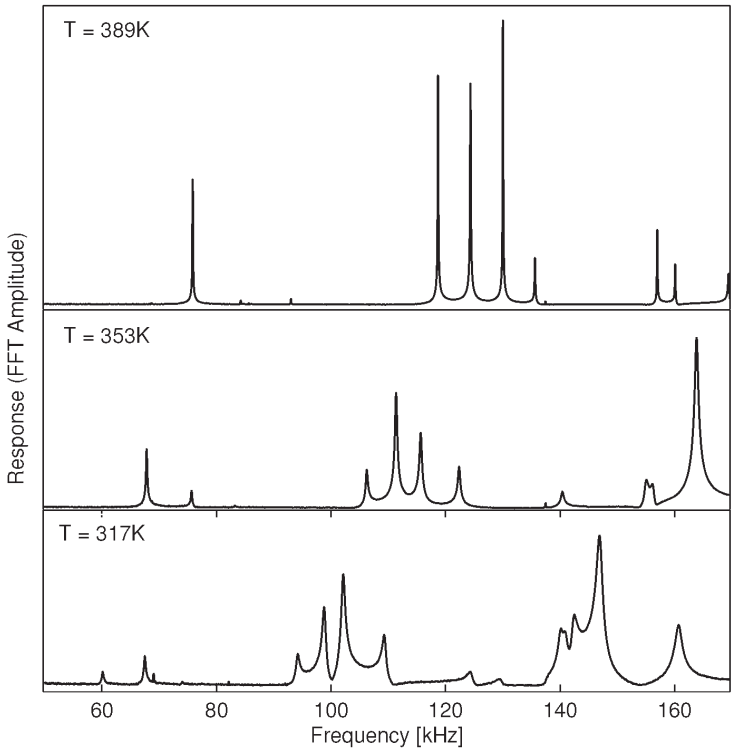

Figure 12: Illustration of the attenuation increase below the Curie point (outputs of the RUS measurements at different temperatures).

of the specimen were recorded during cooling from above the Curie point down to the T_{pM} temperature. The strategy was following:

- At 393K (i.e. safely above the Curie point), the specimen was scanned in the full 20×20 grid to identify accurately the resonant frequencies as well as the shapes of 37 vibrational modes. Such information was sufficient for determination of the c' and c_{44} coefficients.

- Then, the specimen was heated up to 398K, from where the temperature was decreased in successive steps of approximately -5K till a 280K temperature was reached, where further measurements were disabled by water vapor condensation at the faces of the specimen. At each temperature, the surface of the specimen was scanned by a sparse 3×3 grid, which was not sufficient for the identification of the shapes of the vibrational modes, but enabled reliable determination of the spectra.

At 393K, the full scan data were used for determination of the elastic coefficients by the same inverse procedure as applied in section 3.1 to austenite of Cu-Al-Ni, so the results were, again, obtained in a form of linear combinations of elastic coefficients sorted by accuracy. These are listed in Tab.5. Similarly to the case of Cu-Al-Ni (see Tab.1 for comparison), the first combination has nearly exactly the meaning of c', the second of c_{44} and the third of $c_{11} + c_{12}$.

After transforming back from these linear combinations, the reliable results are $c' = (6.9 \pm 0.1)$GPa and $c_{44} = (97.7 \pm 4.7)$GPa, individual values of c_{11}, c_{12} or c_{L} cannot be, naturally, determined. Our aim, however, was the determination of the elastic coefficients

below the Curie point, namely in the vicinity of the premartensitic transitions. As the spectra there were extremely attenuated, only the first few peaks were determinable by fitting the chosen interval of the spectrum by function of form (74), where the parameters A_n, ϕ_n, f_n and FWHM_n were determined by numeric optimization (simplex search method). The analysis was performed in successive steps, starting at the highest temperature (above the Cure point), and then fitting the spectra at lower and lower temperatures. As initial guesses for the search at each temperature, the values obtained in the previous step (i.e. at the previous, higher temperature) were used. This enabled the first two peaks in the spectrum to be accurately traced down through the whole temperature interval (down to $T = 280$K), and four more peaks to be traced down to $T = 353$K (below this temperature, the algorithm was able to localize the peaks and fit the amplitude of the spectrum, but the evaluated phases ϕ_n were not agreeing sufficiently with the experimental results and the FWHMs were not obtainable with sufficient accuracy).

In comparison to the number of resonant frequencies involved in the inverse procedure in the previous cases (up to 100 peaks), such data (two or six peaks) seem to be completely insufficient for the determination of any of the elastic coefficients. However, we can remind us our previous findings about the sensitivity of individual elastic coefficients to individual modes of vibrations for extremely strong cubic anisotropy, according which should the first peaks in the spectrum be nearly explicitly dependent on the c' coefficient only. But how can be such assumption utilized in this case?

If we assume that the shapes of the first few eigenmodes do not change with the temperature ($\alpha_j \neq \alpha_j(T)$), we can express the thermal dependencies of corresponding resonant

k	Combination	C_k^* [GPa]	κ_k [GPa]
1	$0.71c_{11} - 0.71c_{12} + 0.02c_{44}$	12.35	0.01
2	$-0.01c_{11} + 0.02c_{12} + 0.99c_{44}$	98.104	4.72
3	$0.71c_{11} + 0.71c_{12}$	232.32	193.32

Table 5: Combinations of elastic coefficients for the single crystal of austenitic Ni-Mn-Ga above the Curie point.

frequencies as

$$\frac{\partial f_j}{\partial T} = \frac{\alpha_j^{\mathrm{T}} \frac{\partial \Gamma}{\partial T} \alpha_j}{8\pi^2 f_j} = \frac{\alpha_j^{\mathrm{T}} \frac{\partial \Gamma}{\partial C_k} \alpha_j}{8\pi^2 f_j} \frac{\partial C_k}{\partial T}, \tag{75}$$

where the effect of the thermal expansivity is fully neglected. As we have already discussed, the partial derivatives $\partial\Gamma/\partial C_k$ are independent on C_k. For this reason, we can understand (75) as a linear relation between $f_j \frac{\partial f_j}{\partial T}$ (no Einstein's summation law applied) and the thermal derivatives of elastic coefficients. Looking back in Tab.5, we can indubitably assume that the dominant dependence is on c' only[4] and write

$$f_j \frac{\partial f_j}{\partial T} = K_j \frac{\partial c'}{\partial T}, \tag{76}$$

where K_j are constants. Then, with the exact knowledge of c' at some T_0 (the full scan at the temperature above the Curie point) and with thermal dependencies of f_j approximated by differences

$$\left.\frac{\partial f_j}{\partial T}\right|_{T=T_i} \approx \frac{f_j(T_{i+1}) - f_j(T_i)}{T_{i+1} - T_i} \tag{77}$$

we can get an estimate of the change of c' with decreasing temperature

$$\Delta c'(T_k) = \sum_{i=1}^{k} \frac{1}{K_j} f_j(T_i) \frac{f_j(T_{i+1}) - f_j(T_i)}{T_{i+1} - T_i} \tag{78}$$

for every mode (i.e. for every j). In Fig.13, the thermal dependencies of f_j and the corresponding values of $\Delta c'$ are plotted. Near the Curie point, the $\Delta c'$s evaluated for all modes are in an excellent agreement, small divergence appears between $\Delta c'$ determined from mode No.1 and mode No.2 at lower temperatures, which can be ascribed to slight changes of the shapes od the first two modes (i.e. of vectors α_1 and α_2) with the decreasing temperature. However, the difference is still incomparably smaller than the theoretically estimated experimental error of this coefficient (59) for the pulse-echo measurements, so we can suppose that the RUS method here is still more suitable for determination of this coefficient than the pulse-echo methods are.

It is rather complicated to summarize the findings of this subsection into any general conclusion. There is still a lot to be improved within the RUS analysis of Ni-Mn-Ga (or similar) single crystals. Especially the better knowledge of the micromagnetic mechanism of the attenuation is lacking, which might enable us to utilize the RUS results for deeper analysis of this magneto-elastic phenomenon. From the point of view of applicability limits of RUS, we have shown the way how the magneto-elastic attenuation complicates the

[4] Indeed, when expressed numerically, the ratios are

$$\alpha_j^{\mathrm{T}} \frac{\partial \Gamma}{\partial C_1^*} \alpha_j \approx 50 \alpha_j^{\mathrm{T}} \frac{\partial \Gamma}{\partial C_2^*} \alpha_j \approx 5.10^3 \alpha_j^{\mathrm{T}} \frac{\partial \Gamma}{\partial C_3^*} \alpha_j .$$

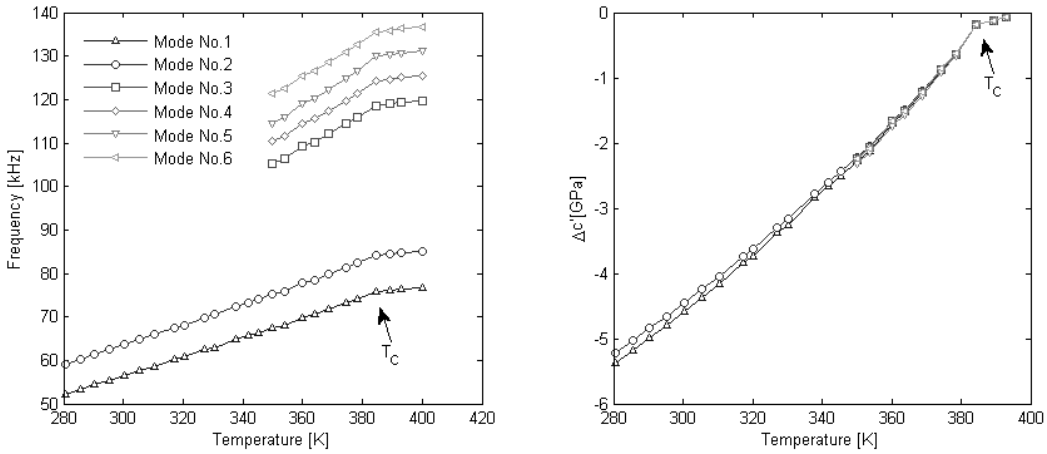

Figure 13: Thermal dependencies of locations of the first six peaks in the spectrum (on the left) and the changes of c' evaluated from them.

determination of elastic coefficients by RUS measurements, in the sense that only first few peaks can be identified far below the Curie point, which precludes reliable determination of all elastic coefficients, especially if the material is as strongly anisotropic as Ni-Mn-Ga. Hereto, it is necessary to point out that no enormous effort was made to analyze thoroughly the spectra (maybe more peaks and their thermal dependencies could have been identified throughout the spectrum) – the aim was to show that the knowledge of the theoretical background of RUS enables us to obtain at least some information on the elastic coefficients, even though the input information is minimal. We have, thus, shown that the knowledge of thermal dependencies of first few resonant frequencies can be sufficient for determination of the one elastic coefficient which is closely related to the corresponding modes.

The RUS analysis of Ni-Mn-Ga single crystals represents here the case when the the applicability of this method is complicated by combination of many different factors (strong anisotropy, significant thermal dependencies of elastic coefficients, temperature-dependent attenuation). Such case illustrates at the same time the main demerit and the strength of the RUS method: Although the nature of the method itself requires sophisticated postprocessing of the experimental data (which must be, moreover, modified for each particular material, etc.), the sought elastic coefficients can be obtained with high accuracy, providing that the resonant spectra contain sufficient information about them.

4 Conclusion

This chapter brings a survey through main ideas of the RUS method for determination of elastic coefficients of anisotropic solids, with a focus on the limitations of this method given by the properties of the examined materials. Throughout the text, at least five essential

questions were open, regarding the applicability a reliability of this method. By formulating these questions explicitly and answering them based on the findings outlined in the chapter, we can summarize the whole content of the text as follows:

Q1. Does the resonant spectrum of free elastic vibrations of a small specimen of known geometry always contain sufficient information on the elasticity of the material? The answer is, surprisingly, not. Some additional information is always required to associate the values of resonant frequencies to individual vibrational modes (see Fig.3 and the discussion around there). This information may have a form of the shapes of the eigenmodes determined by a scanning laser interferometer, or it may by simply brought by very accurate initial guesses of the elastic coefficients, for which the shapes are very similar to the real ones.

Q2. Is there any well-founded way how to estimate the accuracy of the results of RUS? If yes, can this accuracy be improved by increasing the number of frequencies involved in the inverse procedure? Yes, the accuracy can be estimated by formulas like (44), which are following fully from the nature of the method. On the other hand, the increase of the accuracy by involving more and more frequencies in the inverse procedure is not axiomatic. In the example of the wooden rod (see the beginning of subsection 2.3), the ratio between number of frequencies in the spectrum corresponding to the longitudinal and to the torsional modes never exceeds the value $\sqrt{G_\perp/E}$ as the all the higher modes are given only by multiplication (see Fig.2 and the discussion above it) of the lower ones.

Q3. Is the applicability of RUS anyhow limited by the strength of the anisotropy of the examined material? Yes, in some sense. As we have seen both for the single crystals of Cu-Al-Ni (subsection 3.1) and for Ni-Mn-Ga (subsection 3.3), the RUS method is not able to determine accurately the coefficients corresponding to the hardest vibrational modes, if the anisotropy is sufficiently strong. However, as it was shown for both the austenitic phase and the martensitic single variant of Cu-Al-Ni, the RUS measurement can be properly complemented with pulse-echo measurements, which are most suitable for determination of the hardest modes related to the quasi-longitudinal velocities. For extremely weak anisotropy (subsection 3.2), no limitations were found, especially after the RUS measurements were, again, complemented by pulse-echo measurements.

Q4. Is the applicability of RUS anyhow limited by the number of sought independent elastic coefficients? Here, the answer is definitely not (providing that reasonable initial guesses are available). The example of the nanocrystalline copper manufactured by the ECAP method (subsection 3.2) showed that the RUS method can be reliably applied for determination of all 21 elastic coefficients, or even for the detection of the symmetry class of the material. The only problems can be encountered when the material is periodically microstructured (Fig.9), where the microstructure can, at certain frequencies, interfere with the vibrational modes.

Q5. Can the RUS method be easily modified for particular materials with special, more complex properties? Although this question is quite general, we can say that the answer might be yes. The adaptability of RUS was illustrated in subsection 3.2 for the magneto-elastically attenuated single crystal of the Ni-Mn-Ga alloy. The positive answer can be also supported by many of the references listed below. On the other hand, there are many challenging issues for the RUS method not solved yet. Continuously graded material, metallic foams, metamaterials or nanoscale objects are few topic of those to which the RUS community turns now and which will check the real adaptability of this method. The limitations which will be found for such highly advanced applications of RUS cannot be foretold yet.

5 Acknowledgement

Authors would like to great acknowledge V. Novák and P. Šittner (Institute of Physics ASCR, v.v.i.) for providing specimens from CuAlNi, M. Janeček (Faculty of Mathematics and Physics, Charles University) for Cu specimens prepared by ECAP technique, and Simo-Pekka Hannula (Laboratory of Materials Science, Helsinki University of Technology, Finland) for NiMnGa specimens.

The work was supported by the Marie-Curie Research Training Network project MULTIMAT (MRTN-CT-2004 505226), the project No. 101/06/0768 of the Czech Science Foundation, the project A200100627 of the Grant Agency of ASCR, the institutional project of IT ASCR , v.v.i., CEZ:AV0Z20760514, and from the research center 1M06031 of the ministry of education of the Czech Republic.

References

[1] Stekel, A.; Sarrao, J.L.; Bell, T.M.; Lei, M.; Leisure, R.G.; Visscher, W.M.; Migliori, A. J. Acoust. Soc. Am. 1992, Vol.2I, 663–668.

[2] Migliori, A.; Sarrao, J.L.; Visscher, W. M.; Bell, T.M.; Lei, M.; Fisk, Z.; Leisure, R.G. Physica B 1993, Vol.183 (1-2), 1–24.

[3] Willis, F.; Leisure, R.G.; Kanashiro, T. Phys. Rev. B 1996, Vol.54, 9077–9085.

[4] Sarrao, J.L.; Mandrus, D.; Migliori, A.; Fisk, Z.; Bucher, E. Physica B 1994, Vol.199-200, 478–479.

[5] Ulrich, T.J.; Darling, T.W. Geophys. Res. Lett., 2001, Vol.28, 2293–2296.

[6] Kim, Y.H.; Song, S.-J.; Kwon, S.-D.; Cheong, Y.-M.; Jung, H.-K. Ultrasonics 2004, Vol.42, 551–555.

[7] Guo, H.; Lal, A. Proceedings of the IEEE Ultrasonics Symposium 2001, 863–866.

[8] Araki, W.; Kamikozawa, T.; Adachi, T. NDT&E Int. 2008, Vol.41, 82–87.

[9] Li, G.; Lamberton, G.; Gladden, J.R. submitted to Phys. Rev. B.

[10] Fan, Y.; Tysoe, B.; Sim, J.; Mirkhani, K.; Sinclair, A.N.; Honarvar, F.; Sildva, H.;Szecket, A,; Hardwick, R. Ultrasonics 2003, Vol.41, 369–375.

[11] M. K. Fig, MSc Thesis, Montana State University 2005.

[12] Landa, M.; Sedlák, P.; Šittner, P.; Seiner, H.; Novák, V.: Mater. Sci. Eng. A 2007, vol.462, 320–324.

[13] Demarest, H. H. Jr. J. Acoust. Soc. Am. 1971, Vol.49, 768–775.

[14] Ohno I. J. Phys. Earth 1976, Vol.24, 355–379.

[15] Maynard, J. Phys. Today 1996, Vol.49, 26–31.

[16] Sarrao, J.L.; Chen, S.R.; Visscher, W.M.; Lei, M.; Kocks, U.F.; Migliori, A. Rev. Sci. Instrum. 1994, Vol.65, 2139–2140.

[17] Ogi H.; Sato K.; Asada T.; Hirao M. J. Acoust. Soc. Am. 2002, Vol.112, 2553–2557.

[18] Lei, M.; Sarrao, J.L.; Visscher, W.M.; Bell, T.M.; Thompson, J.D.; Migliori, A.; Welp, U.W.; Veal, B.W. Phys. Rev. B 1993, Vol.47, pp. 6154–6156.

[19] Sarrao, J.L.; Mandrus, D.; Migliori, A.; Fisk, Z.; Tanaka, I.; Kojima, H.; Canfield, P.C.; Kodali, P.D. Phys. Rev. B 1994, Vol.50, 13125–13131.

[20] Spoor, P.S.; Maynard, J.D.; Kortan, A.R. Phys. Rev. Lett. 1995, Vol.75, 3462–3465.

[21] Foster, K.; Leisure, R.G.; Shaklee, J.B.; Kim, J.Y.; Kelton, K.F. Phys. Rev. Lett. 1999, Vol. 59, 11132–11135.

[22] Nakamura, N.; Ogi, H.; Hirao, M. Acta Mat. 2004, Vol.52, 765–771.

[23] Ogi, H.; Nakamura, N.; Hirao, M. Fatigue Fract. Eng. M. 2005, Vol.28, 657–663.

[24] Ikeda, R.; Tanei, H.; Nakamura, N.; Ogi, H.; Hirao, M.; Sawabe, A.; Takemoto, M. Diam. Relat. Mater. 2006, Vol.15, 729–734.

[25] Ledbetter, H.; Leisure, R.G.; Migliori, A.; Betts, J.; Ogi, H. J. Appl. Phys. 2004, Vol.96, 6201–6206.

[26] Leisure, R.G.; Foster, K.; Hightower, J.E.; Agosta, D.S. Mater. Sic. Eng. A. 2004, Vol.370, 34–40

[27] Ogi, H.; Fukunaga, M.; Hirao, M., Ledbetter, H. Phys. Rev B 2004, Vol.69, 241041–241048.

[28] Muller, M.; Sutin, A.; Guyer, R.; Talmant, M.; Laugier, P.; Johnson, P.A. 2005 J. Acous. Soc. Am. 2005, Vol. 118, 3946–3952.

[29] Payan, C.; Garnier, V.; Moysan, J.; Johnson, P.A. J. Acous. Soc. Am. 2007, Vol.121, EL125–EL130.

[30] Muller, M.; Tencate, J.A.; Darling, T.W.; Sutin, A.; Guyer, R.A.; Talmant, M.; Laugier, P.; Johnson, P.A. Ultrasonics 2006, Vol.44(SUPPL.), e245–e249

[31] Fung, Y.C.; Tong, P.: Classical and computational solid mechanics. Singapore: World Scientific Publishing, 2001.

[32] Sedlák, P., PhD Thesis, CTU in Prague, 2008.

[33] Yoneda, A. Earth Planets Space 2002, Vol.54, 763–770.

[34] Tian, J.; Ogi, H.; Hirao M. Appl. Phys. Lett. 2005, Vol.87, 204107-1–204107-3.

[35] Radovic, M.; Barsoum, M.W.; Ganguly, A.; Zhen, T.; Finkel, P.; Kalidindi, S.R.; Lara-Curzio, E. Acta Mater. 2006, Vol.54, 2757–2767.

[36] Zadler, B.J., PhD Thesis, Colorado School of Mines, 2005.

[37] Ogi, H.; Ledbetter, H.; Kim, S.; Hirao, M. J. Acoust. Soc. Am. 1992, Vol.106, 660–665.

[38] Sedlák, P.; Seiner, H.; Landa, M.; Novák, V.; Šittner, P.; Manosa, L. Acta Mater., 2005, Vol.53, 3643–3661.

[39] Bhattacharya, K. Microstructure of Martensite, Oxford: Oxford University Press, 2003.

[40] Auld, B.A. Acoustic fields and waves solids, Vol.1, New York: John Wiley and Sons, 1973.

[41] Stipcich, M.; Manosa, L.; Planes A. Phys. Rev. B 2004, Vol.70 054115-1–054115-5.

[42] Bennett, B.W.; Shannette G.W. Acoust. Lett. 1980, Vol.4, 99–104.

[43] Saunders, G.A.; Liu, H.J.; Bach, H. J. Mat. Sci. 1998, Vol.33, 4589–4594.

[44] Kim,H.S.; Ryu W.S.; Janecek, M.; Baik, S. Ch.; Estrin, Y. Adv. Eng Mater. 2005, Vol.7, 43–46.

[45] Kim, H. S. Mater. Sci. and Eng. A 2006, Vol.430, 346–349.

[46] Yoon, S.Ch.; Seo M.H.; Kim, H.S. Scripta Mater. 2006, Vol.55, 159–162.

[47] Kim, H.S.; Estrin, Y. Mater. Sci. Eng. A 2005, Vol.410–411, 285–289.

[48] Landa, M.; Sedlák, P.; Seiner, H.; Heller, L.; Bicanová, L.; Šittner, P.' Novák, V. Accepted to Applied Physics A (2008).

[49] Seiner, H. PhD Thesis, CTU in Prague, 2008.

[50] Seiner, H. Bicanová, L.; Sedlák, P.; Landa, M.; Heller, L.; Hannula, S.-P. submitted to Mater. Sci. Eng. A. (special issue 'Proceedings of 15th ICIFMS 2008').

[51] Rudajevova, A. Kovove Mater. 2008, Vol.46, 71–76.